Evaluation of Nanoporous Carbon Thin Films for Drug Loading and Controlled Release

by

Alpha Labiano

A Thesis Presented in Partial Fulfillment
of the Requirements for the Degree
Master of Science

Approved November 2011 by the
Graduate Supervisory Committee:

Bryan Vogt (Co-chair)
Kaushal Rege (Co-chair)
Lenore Dai
Thrimoorthy Potta

ARIZONA STATE UNIVERSITY

December 2011

ABSTRACT

Mesoporous materials that possess large surface area, tunable pore size, and ordered structures are attractive features for many applications such as adsorption, protein separation, enzyme encapsulation and drug delivery as these materials can be tailored to host different guest molecules. Films provide a model system to understand how the pore orientation impacts the potential for loading and release of selectively sized molecules. This research work aims to develop structure-property relationships to understand how pore size, geometry, and surface hydrophobicity influence the loading and release of drug molecules.

In this study, the pore size is systematically varied by incorporating pore-swelling agent of polystyrene oligomers (hPS) to soft templated mesoporous carbon films fabricated by cooperative assembly of poly(styrene-block-ethylene oxide) (SEO) with phenolic resin. To examine the impact of morphology, different compositions of amphiphilic triblock copolymer templates, poly(ethylene oxide)-block-poly(propylene oxide)-block-poly(ethylene oxide) (PEO-PPO-PEO), are used to form two-dimensional hexagonal and cubic mesostructures. Lastly, the carbonization temperature provides a handle to tune the hydrophobicity of the film.

These mesoporous films are then utilized to understand the uptake and release of a model drug Mitoxantrone dihydrochloride from nanostructured materials. The largest pore size (6nm) mesoporous carbon based on SEO exhibits the largest uptake (3.5μg/cm^2); this is attributed to presence of larger internal volume compared to the other two films. In terms of release, a controlled response is observed for all films with the highest release for the 2nm cubic film (1.45 μg/cm^2) after 15 days, but this is only 56 % of the drug loaded. Additionally,

the surface hydrophobicity impacts the fraction of drug release with a decrease from 78% to 43%, as the films become more hydrophobic when carbonized at higher temperatures. This work provides a model system to understand how pore morphology, size and chemistry influence the drug loading and release for potential implant applications.

For my beloved parents,

to whom I owe everything I am today

ACKNOWLEDGEMENTS

My sincerest gratitude goes to those who have been very instrumental to the completion of this research work and have motivated me all throughout the course of my study.

First of all, I would like to acknowledge my mentor, Dr. Bryan Vogt, for giving me the opportunity to work with his research group. If not for his trust, guidance and willingness to educate students, this study would never have been possible. His natural interests in research, admirable enthusiasm, endless list of ideas, and the urge for in-depth understanding of the science have made me feel how fulfilling the experience is to be back in the academe after several years. He taught me the value of learning, critical thinking, and the passion in doing what you do. Even for this short period of time, he has been a good mentor and I will always be grateful for all that I have learned from him.

Likewise, I would take this opportunity to express my gratitude to my defense committee, Dr. Kaushal Rege, Dr. Lenore Dai, and Dr. Thrimoorthy Potta for giving me this chance to present my work and sparing their time to provide insightful ideas for the work done. It is a pleasure having them as part of my committee.

I also would like to thank my friends and fellow ASU research students, Mingzhi Dai and Jessica Torres, for providing their support and encouragement throughout this period of my life. They have welcomed me during my integration to the group and have constantly helped me through the ins and outs. I will truly miss those times we have spent together in the lab and those usual lunch dates we have shared. To my other groupmates, Todd Prichard and Michael Marrs, thank

you for extending your help to me in any way you can. Also, thanks to the folks from FDC especially to Barry O'Brien for his generous effort on giving me technical guidance and for the help he provided in the surface analysis/materials characterization of my film materials using AFM. To Dr. Rege's research group at the BioLab, I would like to thank them for the countless ways they have shown how supportive and helpful they are. Thanks to Huang-Chiao Huang, David Taylor, Lucas Vu, and Matt Christensen.

To my Fall 2010 batchmates, thanks. They made my first semester in graduate school one of a kind. I have found friends in all of them and made me feel as if I am not million miles away from home. All the moments that we had are worth keeping. Thank you for the friendship. I will always remember this fun, crazy time in sunny Arizona.

Last but not the least, to my family, who have unwavering faith in me and have provided their full support the moment I decided to pursue graduate studies here in the US. Even if we are far apart, they never failed to show how I am truly blessed with such a loving and caring family. In those trying times, I found my refuge in them. They are my life, my inspiration. Thank you for staying with me through these years and sharing this lifelong journey.

TABLE OF CONTENTS

CHAPTER Page

LIST OF FIGURES

Figure Page

Chapter 1

INTRODUCTION

1.A Overview

Mesoporous materials have been extensively researched in the past decades and are of great interest in numerous applications such as separation[1,2], catalysis[3], adsorption, energy storage[4,5], and nanomedicine[6-11], as these materials can be tailored to cater different guest molecules. Due to its stable structure and well-defined surface properties, mesoporous materials are viable in biomedical applications like encapsulation of proteins, enzymes, pharmaceutical drug, and other biologically active molecules[9]. In drug delivery, the selection of carriers for poorly soluble pharmaceuticals is a significant challenge since low water-solubility results in poor absorption and low bioavailability[6], which consequently leads to a diminished therapeutic effect of the drug. However, hydrophobicity and low solubility in water appear to be intrinsic for many drugs since this helps a drug molecule to penetrate the cell membrane and reach critical intracellular targets[6]. As such, one approach is to encapsulate the drug within hydrophobic domains. In addition, it is desirable to have vehicles that are biodegradable, have small particle size, increased bioavailability, possess high loading capacity, demonstrate prolonged circulation, and specifically accumulate in required pathological sites in the body[6-7]. Since ordered mesoporous materials possess favorable features such as large surface area, high pore volume and tunable pore sizes[9-10], which can meet the said requirements; these materials can be used as carriers for drug delivery. Apart from these characteristics, chemical inertness, low toxicity[12] and hydrophobicity are also important factors for DDS, which makes mesoporous carbons as notable drug carriers. Since the internal pore

surfaces of the mesoporous carbons are highly hydrophobic, the efficacy of release of the guest molecules in aqueous solutions is not well understood and thus, need to be addressed. In order to easily investigate these effects, films will be used as a model system. This research work aims to understand how pore size, geometry, and surface hydrophobicity can influence the potential for drug uptake and controlled release of a model drug Mitoxantrone dihydrochloride from templated mesoporous carbon films.

In this introductory chapter, a brief discussion on some of the challenges in drug delivery systems (DDS) are presented to provide an insight on the requirements set for suitable drug carriers and the role of nanotechnology to potentially overcome these challenges in controlled release and targeted delivery[7]. Since materials in the nanometer length scale pose a viable solution, mesoporous materials have been extensively researched and have been employed as drug carriers[9-10]. Previously reported studies related to the application of mesoporous materials in DDS, which take different forms and material types are also cited. Additionally, mesoporous materials' morphological properties such as pore size, geometry, and surface properties can be tuned for specific applications by varying the synthesis conditions. The different synthesis routes for mesoporous carbons, and the different tools and techniques used to characterize these films are also discussed.

In order to accommodate large molecules, the pore size of the mesoporous carbons need tuning and the different synthesis routes to achieve this will be discussed in Chapter 2 which involve templating methods employing amphiphilic block copolymers and pore swelling agents. Several large pore mesoporous materials have been synthesized based upon the surfactant poly(ethylene oxide)-

b-poly(propylene oxide)-b-poly(ethylene oxide) (PEO-PPO-PEO)[13-16], however, limitations abound in directly templating with pore sizes larger than 12nm because of its molecular weight and composition[17]. An alternative route is to template using poly(styrene)-b-poly(ethylene oxide) (PS-b-PEO) with added pore swelling agent homopolymer polystyrene (h-PS) [18] as demonstrated by Deng et al. But this protocol has not been extended to thin films and thus, is investigated to determine impact on the morphology of mesoporous carbon films.

In addition to pore size, structure and surface hydrophobicity are also modified by using different structuring directing-agents during synthesis and varying the carbonization temperatures, respectively. Chapter 3 explores the drug loading capacity and subsequent release behavior of mesoporous carbons films as a function of pore size, film thickness, mesostructure and hydrophobicity. These material characteristics are factors to be considered when defining sustained drug release from porous materials. Controllable pore size allows different size of molecules suitable for drug delivery while an ordered pore network allows fine control of the drug load and release kinetics. Moreover, hydrophobicity of the film can be varied through different carbonization temperatures; the hydrophobicity is an important factor to take into account when designing DDS as this affects the interaction of the materials with the biomembrane[19] and also allows control of the drug loading and release[20].

Conclusions and future work relevant to this study are briefly discussed in Chapter 4. This includes plans for further understanding the factors that influence the loading and release in mesoporous carbon films such as evaluation of additional loading parameters (e.g, loading temperature, shaker speed) to maximize drug loading, release conditions (e.g, temperature, pH of PBS) to

determine performance at different environments, and surface modification by using an alternative method to change hydrophobicity such as nitric acid oxidation. Also, to have a better understanding of the pore size effect on release, it is proposed to run experiments on the mesoporous carbon films templated with SEO (added hPS for pore size variation) to make a more reliable comparative analysis. Another plan being considered is to evaluate the potential of mesoporous carbon films as scaffolds in implant applications such as in tissue engineering.

1.B Drug Delivery Systems

Current efforts in the design of drug delivery systems (DDS) aim to develop new materials that can meet the stringent requirements in the transportation of therapeutic drugs. Some of the key challenges of most DDS are poor bioavailability, solubility, intestinal absorption, sustained and targeted delivery to affected site, therapeutic effectiveness, side effects, and plasma fluctuations which either fall below the minimum effective concentration or exceed the safe therapeutic concentrations[7]. The desire to overcome these challenges emanate from the need to have improved product efficacy wherein maximum response from the drug is achieved as it delivers and maintains the concentration at the precise sites in the body and mitigate the risk to patient's safety[6-9].

The therapeutic effectiveness of any drug is often diminished by its inability to access the site of action in appropriate doses. Conventional methods of administering drugs through oral ingestion or intravascular injection often requires periodic intake as the medication is distributed throughout the body by systemic blood circulation, and thus limit the portion of the drug that reaches the

affected site. Periodic administration by traditional means is also susceptible to variable systemic drug concentrations with alternating periods of ineffectiveness and/or toxicity. Controlled-release drug delivery systems attempt to maintain therapeutic concentration of a drug in the body as it delivers for a prolonged period of time to a targeted site and have a protected drug interaction with the diseased tissue. This holds a great promise in improving drug efficacy and sustaining the required plasma and tissue drug levels in the body and therefore, avoiding any damage to healthy tissues. A comparison of systemic profiles established for conventional drug administration and controlled release is shown in figure 1.1.

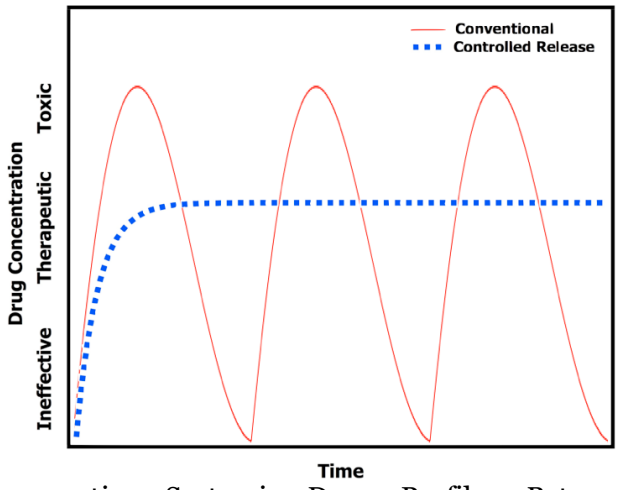

Figure 1.1 Comparative Systemic Drug Profiles Between Conventional Administration and Controlled Release [7]

With the intent of leaning towards development of efficient controlled-release drug delivery systems, the design of appropriate carriers comes at great importance at this point. Nano-based strategies in the design of DDS can potentially overcome the challenges in controlled release and targeted delivery through the development and fabrication of nanostructures at submicron scale and nanoscale[6-10]. Nanostructures have the ability to protect encapsulated drugs

from hydrolytic and enzymatic degradation in the gastrointestinal tract; deliver a wide range of drugs to targeted sites of the body for sustained release and therefore able to deliver drugs, proteins, and genes through peroral administration[7]. These materials can transport drugs that are highly water insoluble; can increase oral bioavailability due to their specialized uptake mechanisms and are able to remain in the blood circulation for prolonged period of time and thus, enable sustained drug release resulting to less plasma fluctuations and minimizing the drug side-effects[7-8]. Unique features such as ordered pore network with homogenous size and functionalized surfaces allows the control of drug loading and release as well as high pore volume and high surface area provides a potential to maximize drug loading capacity[10]. The said capabilities of nanoporous materials are owed to the ability to modify its morphological properties to cater specific applications.

1.C Mesoporous Materials Applications for Drug Delivery Systems

Four decades ago, Le Page and coworkers published an invention addressed to synthesizing porous silicates. Their work presented the ability to synthesize materials with high surface area and porosity by calcining silica gels[24]. Moreover in the 1980s, pillared clays[21-22], had been intensively investigated, but were not appropriate materials to form ordered well-distributed porous materials. In the 1990s, Mobil reported the templated synthesis of two mesoporous silicates, MCM-41 and MCM-48; these were the first reported ordered mesoporous molecular sieves that have subsequently been thoroughly studied by researchers. These materials possess long range ordered framework with uniform mesopores, large surface area, and tunable pore diameters by controlling the synthesis conditions or employing surfactants with different chain

lengths during sample preparation[25]. Since then, numerous research works and innovative solutions had been published in the field of nanomaterials and one of great interest is its application in drug delivery systems.

Several mesoporous materials have been evaluated for pharmacokinetic studies in the forms of templates [26], powders [27], film [28] and nanoparticles [29] to name a few. These studies took advantage of the opportunity in tuning the morphological properties of the mesoporous materials to determine its potential use in biological systems and investigate the factors that can influence its performance. In a study of non-eroding nanoporous platforms for implant applications, Gultepe et al synthesized biocompatible nanoporous coatings of anodic aluminum oxide (AAO, 20nm and 200nm pore diameter) and anodic titanium oxide (ATO, 125nm pore diameter), loaded with model drug Doxorubicin and monitored the release of drug in phosphate-buffered (PBS) saline by in-situ fluorometry[25] technique. Results showed release for ATO is highest at about 45% after 2 weeks while AAO-20 displayed a 30% release and AAO-200 at 20%. Interestingly, the results in the release profile showed lower for the large pore size template but the mechanism of release as a function of pore size was not clearly elucidated. However, the results proved that these systems are able to perform sustained release of the drug. On a research work done on Ibuprofen (IBU) loading and release behavior on ordered mesoporous carbon powders conducted by Wang et al showed that the IBU adsorption amount was primarily a function of the specific area and the pore volume[12]. The amount of drug adsorbed is higher at increasing drug concentration with a maximum amount loaded at nearly 2mmol/g for 120mmol/l of IBU. However, no clear dependency on pore diameter was observed for the analyzed materials in terms of

drug adsorption. The release profile had a two-step release process with an initial burst followed by a slower release, which is frequently observed for most nonfunctionalized matrices[10], reaching approximately 95% of the drug loaded after 60hours. For mesoporous silica films, Suh and co-workers investigated the release kinetics of Rhodamine dyes from 160nm thick films with vertically aligned 9nm accessible pores which adsorbed ~0.67 μg/ per cm^2 with full release in 80 mins for all molecules examined[28]. The drug uptake amount in the film was similar to that observed in mesoporous silica powders but the release kinetics is slower[28] probably related to the fact that the pores in the films as closed near the substrate interface. As these work have shown potential for drug delivery, clearly, there are still some areas that need further understanding as not all systems behave similarly and continuous improvement and development of new materials sets are necessary to meet stringent requirements in drug delivery.

Research works cited above are just a small portion of numerous studies done on this field with different dosage forms and material types. Mesoporous silica nanoparticles (MSN) has been most commonly examined due to its relative ease in synthesis, high surface area, large pore volume, ease of functionalization, biodegradability, and generally low cytotoxicity[9, 29-32]. However, to effectively deliver drug to the targeted pathological site, nanoparticles should be able to remain in the bloodstream for a considerable time without being eliminated from the system. Adjusting the nanoparticle size and its surface characteristics can mitigate this risk. The particle size used in drug delivery system should be large enough to prevent rapid leakage into the blood capillaries but small enough that it can escape capture by fixed macrophages that are present in the reticuloendothelial system, such as the liver and spleen[33]. One of the advantages

of nanoparticles is that their size is tunable and therefore can be tailored depending on specific requirements. From literature, the size of the sinusoid in the spleen and the fenestra of the Kuffer cells in the liver vary from 150 to 200nm[34] and the size of the gap between endothelial cells of the leaky vasculature ranges from 100 to 600nm[35]. Consequently, to be able to reach cancer tumor sites, the size of the nanoparticles should be up to 100nm[33]. Apart from size, nanoparticles should ideally have a hydrophilic surface to escape macrophage capture[36]; this can be achieved by either coating the surface with hydrophilic polymer, such as poly(ethylene glycol) (PEG), protects the particles from opsonization by repelling plasma proteins, or nanoparticles can be formed from block copolymers with hydrophobic and hydrophilic domains[33]. Nanoparticles that satisfy the requirements mentioned above have a greater chance to escape capture from reticuloendothelial system, have the ability to circulate in the bloodstream and have a higher probability of reaching the target site. To cite an example, 130nm fluorescent MSNs with mean pore size of 2nm is surface modified with trihydroxysilylpropyl methylphosphonate (THMP) then loaded with campotothecin (CPT) and delivered into a variety of human cancer cells to induce apoptosis[37]. Surface modification of the nanoparticle reduced the aggregation and increased its stability in aqueous solution which resulted to CPT being contained within the nanoparticles and later released in the hydrophobic regions of the cell compartments to exert the apoptotic effect. Moreover, pore size[38] and geometry[9] impact the drug release rate, as well as surface characteristics[9,20] can influence the kinetics. In particular, surface functionalization with long alkyl chains can control the release pattern attributed to the increased hydrophobic interaction between the guest molecules and the

surface[20]. As surface area and hydrophobicity appear to be critical factors in controlling the release of therapeutic agents, highly ordered mesoporous carbons can be used as drug carriers due to its intrinsic chemical inertness and hydrophobic nature. Moreover, carbon materials have shown higher surface areas[39,41], larger pore volume, and similar/lower cytotoxicity[29,42] level compared to mesoporous silica. Thus, this research work utilized carbons based on the said properties and films as a model system in place of particles to easily probe the impact of pore size, geometry, and surface hydrophobicity to the drug loading and controlled release from templated mesoporous carbon materials.

1.D. Mesoporous Carbon Syntheses

Recently, highly ordered mesoporous carbons (MCs) have drawn more attention because of its well-defined structure, appropriate pore size and high surface area[43]. However, the preparation of mesoporous carbon materials with ordered structures is extremely difficult in solution, due to the high formation energy of C-C bonds[13]. Significant research activity has been undertaken to develop MCs due to its potential for numerous applications such as hydrogen storage, catalysis[3], adsorption, separations, electrochemical double capacitors[44], biosensing, semiconductor and space technologies[13]. Different routes of synthesis have been explored in the recent past and these are categorized as hard templating[39,43] or soft templating[43].

In hard-template synthesis method, the templates served as molds for carbon replication and thus, no significant chemical interactions take place between templates and carbon precursors[43]. Moreover, the resulting frameworks are predetermined by the templates, which have well-defined nanostructures such as ordered nanowire, nanorod, or nanotube arrays[13]. Synthesis of

mesoporous carbon replica can be summarized into the following steps: 1) preparation of mesoporous silica hard-template with well-defined structure through surfactant templating followed by template removal, 2) filling the carbon precursors into the mesoporous silica channels by impregnation or infiltration, 3) solidification and carbonization of the cross-linking framework, and 4) removal of the silica hard template via etching using hydrofluoric acid (HF) or sodium hydroxide (NaOH) solution.[45] Synthesis of self-supported highly ordered carbon materials through template-mediated structures was pioneered by Ryoo, et al (CMK-1) wherein mesoporous silica molecular sieves (MCM-48) served as the hard template. Sucrose was utilized as a carbon precursor, which underwent a carbonization process with a temperature range of 1073-1373K (800-1100°C) using sulfuric acid as catalyst. Finally, removal of the silica framework proceeded by dissolution in aqueous NaOH-ethanol solution resulting to a cubically structured porous carbon material with a 3nm average pore size[14]. A graphical representation of the mesoporous carbon synthesis and the characterization methods used to determine CMK-1 structure and properties is shown in figure 1.2. Since then, many different hard templated MCs have been prepared by using various mesoporous silicas as templates and many other carbon precursors besides sucrose have been utilized, including furfuryl[46] alcohol, phenol-formaldehyde[13,47] and resorcinol-formaldehyde resins[48], ethylene,[49] propylene,[47] acetonitrile[50], and polypyrrole[51], among others. The control of both the internal and external morphology of the carbon products is possible and having well defined performs is a critical step on the synthesis process.

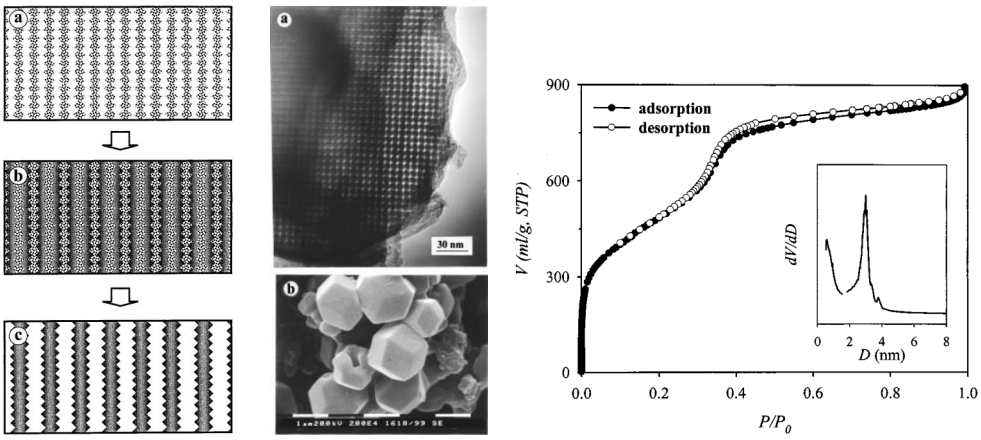

Figure 1.2. (A) CMK-1 synthesis (B) TEM and SEM images of carbon molecular sieve (C) Ar Adsorption-Desorption isotherms with corresponding PSD for hard-templated mesoporous carbon [39]

Conversely, soft-templating involves formation of the nanostructures through self-assembly of organic molecules. There are four key requirements for the successful synthesis of mesoporous carbon materials using soft templates: 1) ability of the precursor materials to self-assemble into nanostructures, 2) presence of at least one template and at least one carbon precursor, 3) thermal stability of the template during curing of the carbon precursor but can readily be decomposed during the carbonization process, and 4) ability of the carbon precursor to form highly crosslinked polymeric material that can retain its nanostructure during the decomposition of the template. The first attempt to fabricate ordered mesoporous carbon was reported by Moriguchi et al., using micelle templates, cetyltrimethylammonium bromide (CTAB)[52], as inspired by MCM-41. Phenolic resin and surfactant self-assembled into disordered mesophases depending upon the surfactant/phenol molar ratio used during the synthesis. The driving force for the self-assembly of the surfactant/phenolic resin complex is proposed as the columbic interaction between the positively charged surfactant head and the negatively charged phenolic resin. However, the

mesophases collapsed after aging at 200°C which eventually resulted to nonporous carbon material. The primary reason for the mesostructural collapse is probably the thermal instability of the lamellar structure upon template removal. Ordered mesoporous carbon film was successfully obtained by Tanaka et al via direct carbonization of an organic-organic nanocomposite utilizing resorcinol/formaldehyde (RF) and triethyl orthoacetate (EOA) as carbon co-precursors and triblock copolymer Pluronic F127 as surfactant; resulting MCs are referred to as COU-1[53] . A relatively recent major advancement in the synthesis of ordered mesoporous carbon frameworks using triblock copolymers poly(ethylene oxide)-b-poly(propylene oxide)-b poly(ethylene oxide) (PEO-PPO-PEO)/resol systems[13] via organic-organic self-assembly was published by Meng and co-workers. Resol is a low molecular weight (~500 g/mol) phenolic resin produced by a catalyzed reaction of phenol and formaldehyde. It is also reported that resols with molecular weights ranging from 200 to 5000 g/mol are suitable carbon precursors to self-assemble with block copolymer and form ordered mesostructures[13]. Upon neutralization with an acid, numerous hydroxyl groups strongly interact with the PEO domains of block copolymer template through hydrogen bonding[13]. Thermopolymerization at temperatures above 100 °C transforms the soluble resols to cross-linked phenolic resins. Thermal treatment at lower temperature (above 350°C) follows resulting to decomposition of the template. After pyrolysis at higher temperature (above 600°C) under inert gas atmosphere, well ordered mesoporous polymer resin and carbon particles with high surface areas and uniform pore sizes are obtained. Figure 1.3 presents a schematic diagram of the synthesis procedure which is summarized as follows: 1) resol precursor synthesis, 2) ordered hybrid mesophases form through organic-

organic self-assembly during solvent evaporation, 3) thermopolymerization of the resols around the template to solidify the framework, 4) template removal at lower temperature (350-600°C) to form mesoporous polymeric resin, and 5) mesoporous carbon through carbonization at higher temperature (600-1200°C). Three factors affect the morphologies of the resulting mesostructures, and these are: 1) volume ratio of PEO to PPO in block polymer surfactants, 2) mixing ratio of carbon precursors to surfactants, and 3) the carbonization conditions.

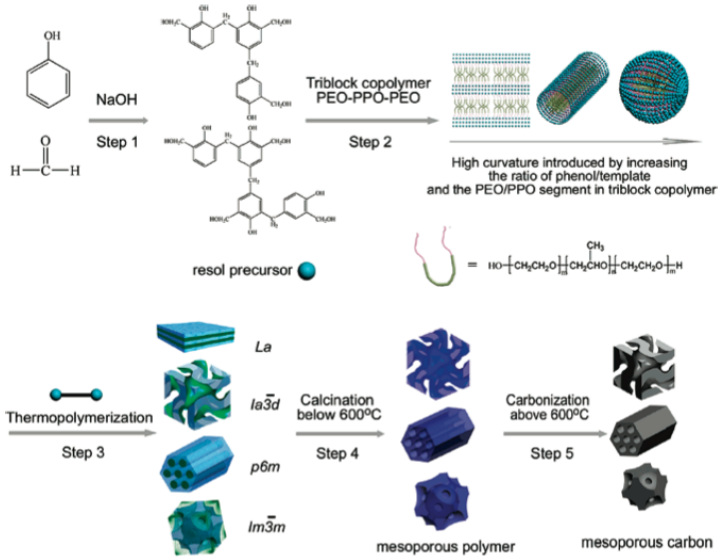

Figure 1.3. Mesoporous Carbon Synthesis thru EISA Method [15]

The existing organic-organic self-assembly method can also be used to cater the need of controlling pore sizes of mesoporous carbons by varying specific parameters in the synthesis pathway such as the amount of precursor materials[13], mass ratios of hybrid nanocomposites[40], structure of surfactants (e.g, relative hydrophilicity of the blocks, molecular weight, etc)[41], processing conditions (eg., aging time, temperature), and addition of pore swelling agents. As large pore sizes are indebted to long hydrophobic chains, varying the composition of the hydrophilic/hydrophobic blocks will be able to increase the hydrophobic volume

which was observed on studies conducted in Pluronic surfactant PEO-PPO-PEO[13]. However, due to limitation in the molecular weight of the commercially available surfactants to enable larger pore sizes, diblock copolymer poly(ethylene oxide)-block-poly(styrene) (PEO-b-PS) was synthesized in lab-scale to customize the hydrophobic block. To further increase the pore size, surfactants coupled with pore swelling agents are also utilized. Studies done by Deng et al on templated (PEO-b-PS) carbon powders suggested that addition of homopolymer polystyrene (h-PS) restrained mesostructural shrinkage and result in thinning of the walls (3.6nm)[18]. The final product exhibits pore size ranging from 22.9-37.4nm for adding 0-20wt% h-PS. The large mesopore sizes were attributed to the pore swelling effect of the low molecular weight h-PS. They proposed a continuous solubilizing process at the core of the PS microdomains resulting to swelling of the hydrophobic core volume. However, excessive addition of h-PS (>20wt%) cannot be homogenously accommodated thus only partial PS microdomains can be filled with more h-PS which then results to wormlike-disordered mesostructure with bimodal/trimodal pore size distribution. The proposed schematics on the formation of the large pores and the transition of the dimensional changes from ordered small pore to disordered large pore mesoporous carbon is shown in figure 1.4.

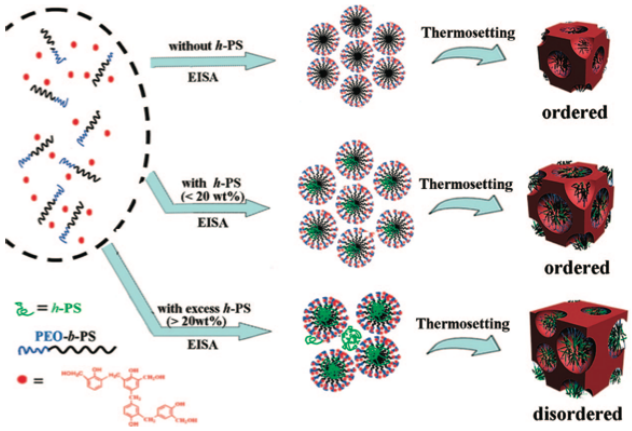

Figure 1.4. Schematic diagram on the formation process of large pore mesoporous carbons by adding homopolymer (h-PS) as pore expander [18]

Even though the frequently used approach to fabricate ordered mesoporous carbon materials is a nanocasting procedure which utilizes mesoporous silicate as a hard template, it is an obviously intricate, high-cost, and thus industrially infeasible method. Therefore, a soft supramolecular self-assembly approach toward ordered mesoporous carbons with open frameworks is desirable and will be use for the purpose of this study.

Mesoporous carbon materials utilized for this research work are synthesized through organic-organic self-assembly of block copolymer templates with phenolic resin. First, the pore size is systematically varied by incorporating pore-swelling agent of polystyrene oligomers (hPS) to soft templated mesoporous carbon films fabricated by cooperative assembly of poly(styrene-block-ethylene oxide) (SEO) with phenolic resin. To examine the impact of morphology, different compositions of amphiphilic triblock copolymer templates, poly(ethylene oxide)-block-poly(propylene oxide)-block-poly(ethylene oxide) (PEO-PPO-PEO), are used to form two-dimensional hexagonal and cubic mesostructures. Lastly, the carbonization temperature provides a handle to tune

the hydrophobicity of the film. A graphical overview of the process is shown in figure 1.5. Details of the preparation method will be discussed in the succeeding chapters.

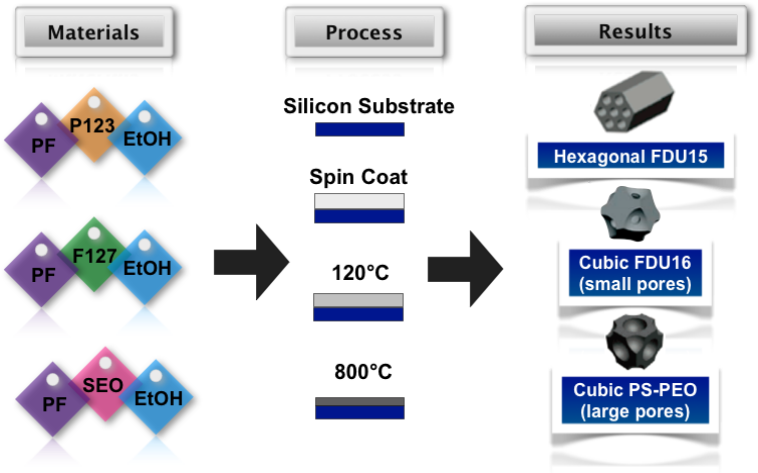

Figure 1.5. Schematic diagram of the process overview for the synthesis of the mesoporous carbon films. Phenol-Formaldehyde Resin (PF), Surfactants (Pluronic PEO_x-PPO_x-PEO_x (P123, F127) and SEO), and solvent ethanol (EtOH).

1.E. Materials Characterization

1.E.1 Determination of Optical Properties through Ellipsometry

Ellipsometry is a non-destructive, contactless optical technique used for the investigation of the optical properties of thin films. It is a very sensitive metrology tool that provides unparalleled capabilities for thin film metrology. This is commonly used to characterize film thickness for single layers or complex multilayer stacks ranging from angstrom to micrometer scale length. This technique do not directly measure the thickness or optical properties of the film, instead, it measures the change of polarization upon reflection or transmission. The polarization change is directed by the specimen's properties and the detected values are typically analyzed through model fits. An illustrative schematic of an ellipsometry experimental setup is shown in Figure 1.6.

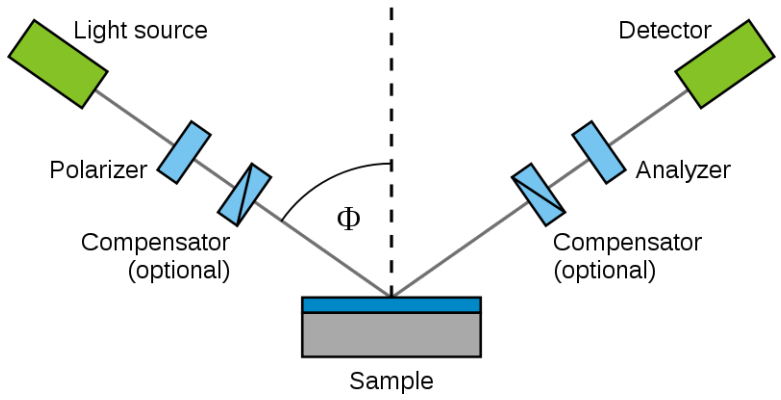

Figure 1.6. Schematic illustration of the spectroscopic ellipsometer used to determine the film thickness

Light passes through the polarizer producing a linear polarized radiation which falls into the sample surface. The reflected beam, which is elliptically polarized, then passes through the analyzer. The change in polarization is measured through the ellipsometric angles, Ψ and Δ, describing the amplitude ratio and the phase difference.

In addition to film thickness, porosity and pore size distribution (PSD) of thin porous films can be estimated with the aid of ellipsometric porosimetry (EP). The method is based on ability of a porous film to condense solvent vapor inside the pores that is dependent upon the pore size as defined by capillary condensation. Such adsorption is performed in a vacuum chamber and monitored by ellipsometry. The solvent for adsorption is desired to have: a) low contact angle with the porous film being analyzed to be able to penetrate into the pores, b) a boiling temperature higher than the ambient, to be able to condense at room temperature, but not significantly higher to provide substantial saturated pressure and c) no chemical interaction with the porous film. Toluene is used as a solvent for adsorption in porous films as its properties meet the requirements of

EP. It has a boiling temperature of 110.6°C, saturated vapor pressure of approximately 24 torr at room temperature, and low contact angle (<5deg) with all studied materials. Additionally, toluene molecule is non-polar and thus reduces interaction with pore walls.

The experimental setup is illustrated in figure 1.7 wherein a porous film on a silicon substrate is placed inside a vacuum chamber equipped with ellipsometer and mass flow controllers (MKS) for the toluene vapor and dry air streams. Initially, the chamber is at low vacuum and then slowly filled with toluene vapor as it reaches the saturated pressure. Upon reaching saturation point, the chamber is pumped down to low vacuum to undergo desorption of toluene in the porous film. Both the adsorption and desorption processes are monitored in-situ. Results of the experimental measurements are dependencies of ellipsometric angles Ψ and Δ on toluene pressure. The pressure is expressed in relative units (P/Po, where Po is the saturated toluene pressure at room temperature) from 0 to 1. The optical properties and thickness of the film are extracted using model-based analysis and then used in calculation of porosity and pore size distribution.

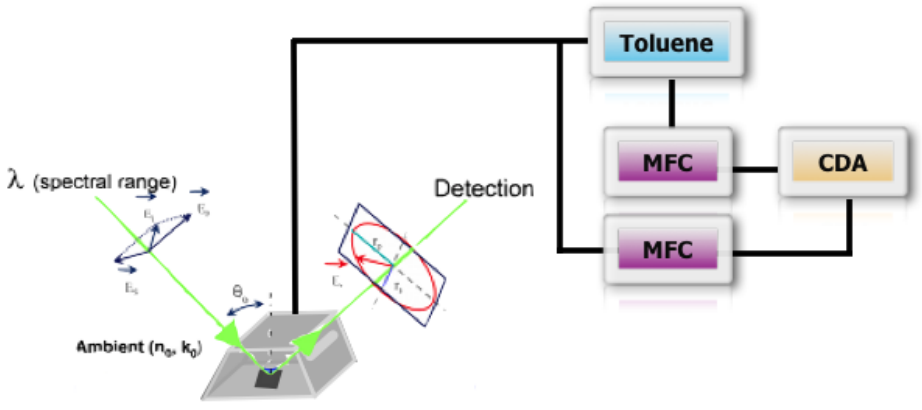

Figure 1.7. Experimental setup for ellipsometric porosimetry

Film porosity can be quantified from the film refractive index measured prior to adsorption and after the film is completely filled with toluene at saturated pressure using the Bruggemann Effective Medium Approximation (BEMA) assuming that all pores were filled after toluene exposure and only two phases exist, amorphous carbon and voids. This can be represented by equation (1).

$$P = \frac{\frac{n_{sat}^2 - 1}{n_{sat}^2 + 2} - \frac{n_0^2 - 1}{n_0^2 + 2}}{\frac{n_{tol}^2 - 1}{n_{tol}^2 + 2}} \qquad (1)$$

From this, effective refractive indices of the empty film (n_o) and the film filled with toluene (n_{sat}) are measured while the refractive index of toluene is well-known (n_{tol} = 1.4961 at 632.8nm at room temperature).

Pore size distribution is calculated from the adsorption and desorption isotherms which is the amount of toluene adsorbed/desorbed in a porous film as a function of relative pressure. Toluene is condensed in the pores at pressures below saturation (P_o) because pressure in liquid below a concave meniscus is lower than that below flat surface. The meniscus curvature radius r_k and the relative pressure P/P_o are related by the Kelvin equation:

$$\ln \frac{P}{P_0} = \frac{2\gamma V_m}{r_k RT} \qquad (2)$$

where R is the universal gas constant, T is temperature in K, γ and V_m are the surface tension and the molar volume of the liquid, respectively. To quantify the pore size distribution, the radius of the pore r_p is calculated with the Kelvin equation using $r_p = r_k + t$, where r_k is the Kelvin radius and t is the thickness of

the absorbed layer on the pore wall before capillary condensation occurs in the mesopore. t is defined by the BET equation, based upon the adsorption of the same adsorptive on a nonporous sample. [54]

1.E.2 Structure via X-ray Diffraction

X-ray diffraction (XRD) techniques can be applied for various purposes ranging from primary sample identification to complex structure determination. The information obtained from these techniques gives a robust image of crystallographic structure and chemical composition of materials and thin films. For this study, XRD was utilized to determine if the synthesized films possess an ordered structure upon thermopolymerization (as-made) and post-carbonization process. This non-destructive analysis technique is based on the measurement of the intensity of the reflected X-ray as a function of the angle between incident and scattered radiation, wavelength or energy as expressed according to Bragg's law, $n\lambda = 2d\sin\theta$, wherein n is an integer, λ is the wavelength of incident wave, d is the interplanar spacing in the atomic lattice, and θ is the angle between the incident ray and the scattering planes.

As illustrated in Figure 1.8, two subatomic particle waves with identical wavelength and phase approach a crystalline sample and are scattered off two different atoms from lattice planes separated by the interplanar distance d. The lower beam traverses an additional length of $2d\sin\theta$. The two elastically diffracted waves from the different atoms interfere constructively resulting in a diffraction pattern in which the intensities and position are directly related to the atomic distribution and distances.

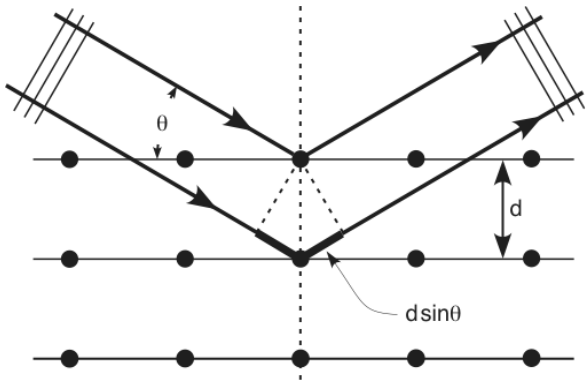

Figure 1.8. Bragg diffraction from a cubic crystal lattice [55]

1.E.3 Surface Topology through Atomic Force Microscopy

The atomic force microscope (AFM) is a very high resolution type of scanning probe microscope which is an excellent metrology tool used for imaging, measuring, and manipulating matter at the nanoscale. It can also provide a three-dimensional surface profile. This was used to characterize the synthesized mesoporous carbon's surface topology and to avoid damage on the sample, intermittent contact or tapping mode was employed. Operation under this condition, the cantilever is driven to oscillate at close proximity to the surface near its resonance frequency by a small piezoelectric element located in the AFM tip holder. As the tip gets near the surface, interacting forces cause a decrease on the oscillation amplitude and to maintain this parameter, the feedback loop adjusts the distance between the tip and surface as the cantilever is scanned over the sample. The force of the intermittent contacts between the tip and sample surface is measured by a laser beam and reflected to a photodiode detector which converts the signal and reports back an AFM image. Schematic of the operating setup is depicted in figure 1.9.

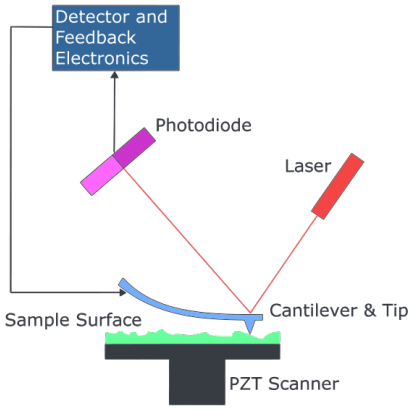

Figure 1.9. Block diagram of Atomic Force Microscope

AFM images of the samples from the experiments are acquired at ambient conditions in intermittent contact or tapping mode. The resulting data are processed using XEI software (Park Systems) which include capability for dimensional analysis of the pore size on the SO films. A sample three-dimensional AFM image of a carbonized SO is shown in figure 1.10.

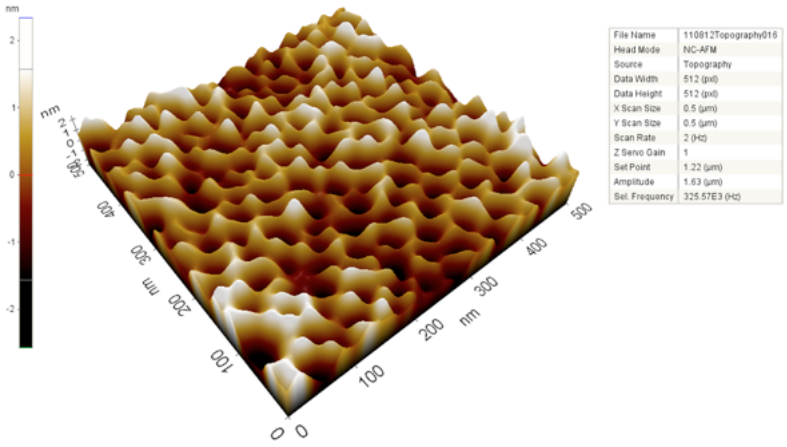

Figure 1.10. AFM micrograph of an approximately 50nm thick SO film pyrolyzed at 800°C with a scan size of 500nm by 500nm, scan rate of 2Hz, and amplitude of 1.63µm.

1.E.4 Analysis of Drug Loading and Release

In drug adsorption and release studies, the use of spectrophotometric techniques is often utilized. This is a quantitative measurement of the reflection or transmission properties of a certain material as a function of wavelength which deals with visible light, near-ultraviolet, and near-infrared. This is commonly used for solutions, transparent or opaque liquids. Prior the actual experiment, calibration curves are generated based upon the absorbance intensity of the analyte as a function of the concentration of the standard solutions. This usually yields a linear equation that is used to calculate concentrations of the solutions at any given time. In a typical drug loading study, samples are incubated in a solution and concentrations are monitored prior and post a specific time period. After which, release studies are subsequently performed normally in a phosphate buffered solution (PBS) solution maintained at 37°C to simulate human's bodily fluids and environment. Figures 1.11 and 1.12 shows an overview of the process and a release experimental setup used for this study.

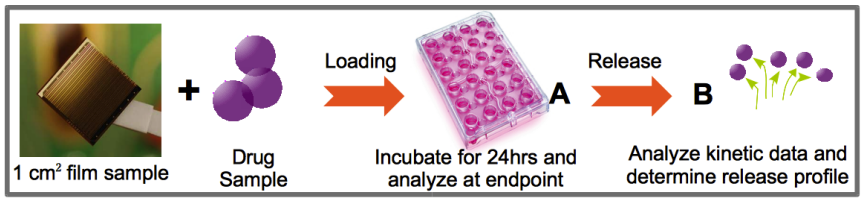

Figure 1.11. Schematic of the drug loading and release process flow

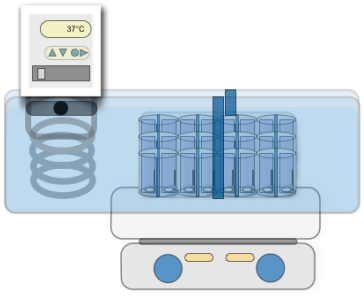

Figure 1.12. Experimental setup for the release study on mesoporous carbon films in a PBS solution maintained at 37°C.

1.F. References

1. Chen, L., Zhu, G., Zhang, D., Zhao, H., Guo, M., Shi, W., Qiu, S. Novel mesoporous silica spheres with ultra-large pore sizes and their application in protein separation *J. Mater. Chem.* **2009** , 19, 2013-2017.

2. Yiu, H., Botting, C., Botting, N., & Wright, P., Size selective protein adsorption on thiol-functionalised SBA-15 mesoporous molecular sieve *Phys. Chem. Chem. Phys.,* **2001**, 3 , 2983-2985.

3. Wang, W., Wang, Y., Shi, H., Liu, H., Song, W. Self-assembled mesoporous carbon films for platinum metal catalyst loading *Thin Solid Films* **2010**, 518, 3604–3609

4. Zhou, J., He, J., Zhang, C., Wang, T., Sun, D., Di, Z., & Wang, D. Mesoporous carbon spheres with uniformly penetrating channels and their use as a supercapacitor electrode material. *Materials Characterization* **2010**, 61(1), 31-38.

5. Yuan, D-S., Zeng, J., Chen, J., Liu, Y. Highly Ordered Mesoporous Carbon Synthesized via in Situ Template for Supercapacitors *Int. J. Electrochem. Sci.,* **2009**, 4, 562 – 570

6. Torchilin, V. P. Nanoparticulates as drug carriers. Imperial College Press, 2006. London.

7. Ochekpe, N. A., Olorunfemi, P. O., & C, N. Nanotechnology and Drug Delivery Part 1 : Background and Applications. *Tropical Jounal of Pharmaceutical Research* **2009**, *8*, 265-274.

8. Paolino, D., et.al., *Drug Delivery Systems*. Encyclopedia of Medical Devices and Instrumentation, Second Edition, 2006 John Wiley & Sons, Inc.

9. Wang, S. Ordered mesoporous materials for drug delivery *Microporous and Mesoporous Materials* **2009**, 117, 1–9.

10. Vallet-Regí, M., Balas, F. and Arcos, D. Mesoporous Materials for Drug Delivery. Angewandte Chemie International Edition **2007**, 46: 7548–7558

11. S.M. Moghimi, A.C. Hunter, and T.L. Andresen Factors Controlling Nanoparticle Pharmacokinetics: An Integrated Analysis and Perspective Annual Review of Pharmacology and Toxicology **2012**, 52, 481-503.

12. Fang, Y., Gu, D., Zou, Y., Wu, Z., Li, F., Che, R., Deng, Y., Tu, B. and Zhao, D., A Low-Concentration Hydrothermal Synthesis of Biocompatible Ordered Mesoporous Carbon Nanospheres with Tunable and Uniform Size. Angewandte Chemie International Edition, **2010**, 49: 7987–7991.

13. Meng, Y., Gu, D., Zhang, F., Shi, Y., Cheng, L., Feng, D., Wu, Z., Chen, Z., Wan, Y., Stein, A., Zhao, D. A Family of Highly Ordered Mesoporous Polymer Resin and Carbon Structures from Organic-Organic Self-Assembly Chem. Mater. **2006**, 18, 4447-4464

14. Zhao, D., Feng, J., Huo, Q., Melosh, N., Fredrickson, G., Chmelka, B., Stucky, G. Triblock Copolymer Syntheses of Mesoporous Silica with Periodic 50 to 300 Angstrom Pores *Science* **1998**, 297, 548-552.

15. Zhao, D.; Huo, Q.; Feng, J.; Chmelka, B. F.; Stucky, G. D. Nonionic Triblock and Star Diblock Copolymer and Oligomeric Surfactant Syntheses of Highly Ordered, Hydrothermally Stable, Mesoporous Silica Structures *J. Am. Chem. Soc.* **1998**, *120*, 6024

16. Fan, J.; Yu, C.; Lei, J.; Zhang, Q.; Li, T.; Tu, B.; Zhou, W.; Zhao, D.Low-Temperature Strategy to Synthesize Highly Ordered Mesoporous Silicas with Very Large Pores *J. Am. Chem. Soc.* **2005**, *127*, 10794.

17. Deng, Y., Yu, T., Wan, Y., Shi, Y., Meng, Y., Gu, D., Zhang, L., Huang, Y., Liu, C., Wu, X., Zhao, D. Ordered Mesoporous Silicas and Carbons with Large Accessible Pores Templated from Amphiphilic Diblock Copolymer Poly(ethylene oxide)-b-polystyrene *J. Am. Chem. Soc.* **2007**, 129, 1690-1697.

18. Deng, Y., Liu, J., Liu, C., Gu, D., Sun, Z., Wei, J., Zhang, J., Zhang, L., Tu, B., Zhao, D. Ultra-Large-Pore Mesoporous Carbons Templated from Poly(ethylene oxide)-b-Polystyrene Diblock Copolymer by Adding Polystyrene Homopolymer as a Pore *Expander Chemistry of Materials* **2008**, 20, 7281–7286

19. Li, Y., Chen, X. & Gu, N. Computational investigation of interaction between nanoparticles and membranes: hydrophobic/hydrophilic effect. *The Journal of Physical Chemistry B* **2008,** 112, 16647-16653.

20. Doadrio, J. C., Sousa, E. M. B., Izquierdo-Barba, I., Doadrio, A. L., Perez-Pariente, J., & Vallet-Regí, M. Functionalization of mesoporous materials with long alkyl chains as a strategy for controlling drug delivery pattern. *Journal of Materials Chemistry* **2006**, *16*(5), 462.

21. Wan, Y. & Zhao, D. On the controllable soft-templating approach to mesoporous silicates. *Chemical Reviews* **2007**, 107, 2821-2860.

22. Corma, A. From Microporous to Mesoporous Molecular Sieve Materials and Their Use in Catalysis. *Chemical Reviews* **1997**, 97, 2373-2420.

23. Farrell, S., Hesketh, R., Savelski, M., Slater, C. Fundamentals, Design and Applications of Drug Delivery Systems *American Society for Engineering Education Annual Conference and Exposition* **2003,** Session 1313

24. Le Page, M., Beau, R. Duchene, J., Porous silica particles containing a crystallized phase and method Application No. US 3493341D A filed on 23-Jan-1967; Publication No. US 3493341 A published on 03-Feb-1970

25. Beck, J. S., Vartuli, J. C., Roth, W. J., Leonowicz, M. E. Kresge, C. T., Schmitt, K. D., Chu, C. T. W., Olson, D. H., Sheppard, E. W. A new family of mesoporous molecular sieves prepared with liquid crystal templates *Journal of the American Chemical Society* **1992** 114 (27), 10834-10843.

26. Gultepe E, Nagesha D, Casse BD, Banyal R, Fitchorov T, Karma A, Amiji M, Sridhar S. Sustained Drug Release from Non-eroding Nanoporous Templates *Small* **2010**, 6, 213-216

27. Wang , X., Liu, P., Tian, Y., Ordered mesoporous carbons for ibuprofen drug loading and release behavior *Microporous and Mesoporous Materials* **2011**, 142, 334–340

28. Suh, M., Lee, H., Park, J., Lee, U., Kwon, Y., Kim, D. A Mesoporous Silica Thin Film as Uptake Host for Guest Molecules with Retarded Release Kinetics *Chem Phys Chem* **2008**, 9, 1402 – 1408

29. Si-Han Wu, Yann Hung and Chung-Yuan Mou Mesoporous silica nanoparticles as nanocarriers Chem. Commun**.**, **2011**, **47**

30. Brian G. Trewyn, Supratim Giri, Igor I. Slowing and Victor S.-Y. Lin Mesoporous silica nanoparticle based controlled release, drug delivery, and biosensor systems *Chem. Commun*., **2007**, 3236–3245

31. Tsai, C.-P.; Chen, C.-Y.; Hung, Y.; Chang, F.-H.; Mou, C.-Y. Monoclonal Antibody-Functionalized Mesoporous Silica Nanoparticles (MSN) for Selective Targeting Breast Cancer Cells. *J. Mater. Chem*. **2009**, 19, 5737–5743.

32. Cheng, S.-H.; Lee, C.-H.; Chen, M.-C.; Souris, J. S.; Tseng, F.- G.; Yang, C.-S.; Mou, C.-Y.; Chen, C.-T.; Lo, L.-W. Tri-Functionalization of Mesoporous Silica Nanoparticles for Comprehensive Cancer Theranostics-the Trio of Imaging, Targeting and Therapy. *J. Mater. Chem*. 2010, 20, 6149-6157

33. Cho, K., Wang, X., Nie, S., Chen, Z., and Shin, D. Therapeutic Nanoparticles for Drug Delivery in Cancer *Clin Cancer Res* **2008**, 14(5), 1310-1316.

34. Wisse E, Braet F, Luo D, et al. Structure and function of sinusoidal lining cells in the liver. *Toxicol Pathol* **1996**, 24, 100-111.

35. Yuan F, Dellian M, Fukumura D, et al. Vascular permeability in a human tumor xenograft: molecular size dependence and cutoff size. *Cancer Res* **1995**, 55, 3752-3756.

36. Moghimi SM, Szebeni J. Stealth liposomes and long circulating nanoparticles: critical issues in phar- macokinetics, opsonization and protein-binding properties. *Prog Lipid Res* **2003**, 42, 463-478.

37. Lu, J., Liong, M., Zink, J., Tamanoi, F. Mesoporous Silica Nanoparticles as a Delivery System for Hydrophobic Anticancer Drugs. *Small* **2007**, 3, 1341–1346.

38. Horcajada P, Ramila A, Perez-Pariente J, Vallet-Regi M. Influence of pore size of MCM-41 matrices on drug delivery rate. Microporous and Mesoporous Materials **2004** , 68, 105-109.

39. Ryoo, R., Hoon Joo, S., Jun, S. Synthesis of Highly Ordered Carbon Molecular Sieves via Template-Mediated Structural Transformation The *Journal of Physical Chemistry B* **1999**, 103 (37), 7743-7746.

40. Pan, K., Zhou, W., Tian, G., Pan, Q., Tian, C., Xie, T., Dong, Y., Wang, D., Fu, H. Dye-Sensitized Solar Cells Based on Large-Pore Mesoporous TiO2 with Controllable Pore Diameters *European Journal of Inorganic Chemistry* **2011**, 30, 4730-4737.

41. Lu, R., Shi, Y., Wan, Y., Weng, Y., Zhang, F., Gu, D., Chen, Z., Tu, B., Zhao, D. Triconstituent Co-assembly to Ordered Mesostructured Polymer-Silica and Carbon-Silica Nanocomposites and Large-Pore Mesoporous Carbons with High Surface Areas *J. Am. Chem. Soc.* **2006**, 128, 11652-11662.

42. Tian Yu, Alexander Malugin, and Hamidreza Ghandehar Impact of Silica Nanoparticle Design on Cellular Toxicity and Hemolytic Activity *ACS Nano*, **2011**, 5 (7), pp 5717–5728

43. Liang, C.; Li, Z.; Dai, S. Mesoporous carbon materials: Synthesis and modification. *Angewandte Chemie-International Edition* **2008,** *47* (20), 3696-3717.

44. Lee, J.; Yoon, S.; Hyeon, T.; Oh, S. M.; Kim, K. B. Synthesis of a new mesoporous carbon and its application to electrochemical double-layer capacitorsChem. Commun.**1999**, 2177.

45. Ryoo, R.; Joo, S. H.; Kruk, M.; Jaroniec, M. Ordered mesoporous carbons. *Advanced Materials* **2001,** *13* (9), 677-681.

46. Wang, X., Bozhilov, K.N. & Feng, P. Facile Preparation of Hierarchically Porous Carbon Monoliths with Well-Ordered Mesostructures. *Chemistry of Materials* **18**, 6373-6381 (2006).

47. Zakhidov, A.A. et al. Carbon Structures with Three-Dimensional Periodicity at Optical Wavelengths. *Science* **282**, 897-901 (1998).

48. Lee, K.T., Lytle, J.C., Ergang, N.S., Oh, S.M. & Stein, A. Synthesis and Rate Performance of Monolithic Macroporous Carbon Electrodes for Lithium-Ion Secondary Batteries. *Advanced Functional Materials* **15**, 547-556 (2005)

49. Yang, Z., Xia, Y., Sun, X. & Mokaya, R. Preparation and hydrogen storage properties of zeolite-templated carbon materials nanocast via chemical vapor deposition: effect of the zeolite template and nitrogen doping. *The Journal of Physical Chemistry B* **110**, 18424-18431 (2006).

50. Xia, Y. & Mokaya, R. Generalized and Facile Synthesis Approach to N-Doped Highly Graphitic Mesoporous Carbon Materials. *Chemistry of Materials***17**, 1553-1560 (2005).

51. Yang, C.-M., Weidenthaler, C., Spliethoff, B., Mayanna, M. & Schüth, F. Facile Template Synthesis of Ordered Mesoporous Carbon with Polypyrrole as Carbon Precursor. *Chemistry of Materials* **17**, 355-358 (2005).

52. Moriguchi, I.; Ozono, A.; Mikuriya, K.; Teraoka, Y.; Kagawa, S.; Kodama, M. Micelle-templated mesophases of phenol-formaldehyde polymer. *Chemistry Letters* **1999,** (11), 1171-1172.

53. Tanaka, S.; Nishiyama, N.; Egashira, Y.; Ueyama, K. Synthesis of ordered mesoporous carbons with channel structure from an organic-organic nanocomposite. *Chemical Communications* **2005,** (16), 2125-2127.

54. Baklanov, M. R., Mogilnikov, K. P., Polovinkin, V. G., Dultsev, F. N. Determination of pore size distribution in thin films by ellipsometric porosimetry *Journal of Vacuum Science & Technology B* **2000**, 18, 1385-1391

55. Hadmack, M. Bragg diffraction from a cubic crystal lattice http://en.wikipedia.org/wiki/File:Bragg_diffraction.png Downloaded 18 October 2011.

Chapter 2

IMPACT OF HOMOPOLYMER PORE EXPANDER ON THE MORPHOLOGY OF MESOPOROUS CARBON FILMS USING ORGANIC-ORGANIC SELF-ASSEMBLY

2.A. Introduction

Ordered mesoporous materials with large surface area and tunable pore sizes are highly attractive for a host of applications[1-3] including adsorption,[4] protein separation,[5] catalysis,[6] enzyme encapsulation[7] due to well-defined pore size of these materials being commensurate with large organic molecules. Templated syntheses using surfactants[8,9] or colloids[10] provide a facile route to fabricate mesoporous materials with a vast array of chemistries.[2,11,12] One framework of particular interest is carbon as it is electrically conductive and chemically inert. Initial fabrication of ordered mesoporous carbon relied on hard templating approaches where an inorganic framework, typically silica, is filled with carbonizable precursors, carbonized and then the inorganic template is etched to yield a negative replica.[13,14] However, this procedure is time consuming and a more direct route would be desired to decrease the synthesis cost. To overcome this tedious procedure associated with hard templating, several soft templating routes have been developed where organic-organic assembly of a carbonizable precursor with a surfactant directly yields a mesoporous carbon upon pyrolysis.[15-17] In particular, the cooperative assembly of pluronic surfactants with oligomeric phenol-formaldehyde resins (resol) provides a robust route to a family of mesoporous carbon powders[18] that is readily extendable to analogous films[19] provided mechanical[20] and interfacial[21] effects are considered. For many applications of mesoporous carbon, the pore sizes obtained from the pluronic

family (~1-4 nm) are desired; however these mesoporous carbons might not be effective for electrochemical sensing of larger molecules such as proteins that are unable to readily fit into these smaller mesopores.[5] Moreover, Zhao and coworkers have recently reported on free standing mesoporous carbons[22] that could be useful filtration membranes, but as resistance scales inversely with pore size it may be advantageous to utilize larger pores. Interestingly, the first templated mesoporous carbon films actually utilized a block copolymer along with a solvent annealing step to yield vertically aligned cylindrical mesopores with larger pore size;[23] however, this procedure is time consuming with solvent anneal and requires exposure of formaldehyde vapors to crosslink the carbonizable precursor. For powders, large pores (>20 nm) have been obtained by using resol and an amphiphilic block copolymer template.[24]

However, these larger templates generally require custom synthesis and thus it is desirable to be able to obtain a range of pore sizes from a single template. For inorganic metal oxide frameworks, expansion in the pore size ranges of the templated materials can be achieved by incorporation of pore-swelling agents such as n-alkanes,[25,26] 1,3,5-tri-methylbenzene (TMB),[27] or triisopropylbenzene.[28] These co-solvents accumulate in the hydrophobic domain of the surfactant assembly, thereby increasing the pore size. However in these cases, a rigid cross-linked network is obtained, which locks the mesostructure in place before the co-solvent can evaporate. For the synthesis of mesoporous carbons, the carbon precursor is generally polymeric and locking an enlarged pore size obtained from volatile solvent swelling is difficult at best. An alternative route to swelling of templated mesoporous carbons was demonstrated by Deng et al. using a poly(ethylene oxide-block-styrene), PEO-b-PS, template with added

homopolymer polystyrene (h-PS).[24] The addition of h-PS increases the hydrophobic domain size and also restrained mesostructural shrinkage. The pore size can be increased from 23 nm to 37 nm by the addition of 20 wt% h-PS. Excessive h-PS (>20 wt%) cannot be contained within the ordered PS domains and loss of ordering with a significant broadening of the pore size distribution is observed. However, the extension of this protocol to thin films has not been examined; significant differences might be expected on the basis of interfacial effects in the resol-pluronic system for thin films.[21]

In this work, we investigate the impact of addition of low molecular weight polystyrene on the morphology of PS-b-PEO templated mesoporous carbon films. A low molecular mass oligomer of PS is utilized to maintain a 'wet' brush during the swelling of the PS domains with up to 20 wt% added. The morphology of the films is examined as a function of the PS concentration in the template solution using ellipsometry to estimate the porosity and pore size distribution, atomic force microscopy (AFM) for the surface morphology, cross-sectional TEM for through plane structure, and grazing incidence small angle x-ray scattering (GISAXS). At low loadings, the added PS does not significantly alter the morphology or pore size; while the pore size distribution broadens at 10 wt % PS with a substantial increase in average pore size. These results are distinct from those previously reported for mesoporous carbon powers,[24] further illustrating the importance of interfaces in soft templated mesoporous carbon films.

2.B. Experimental Section

2.B.1 Materials

Resol, a low molecular weight phenolic resin, was used as the carbon precursor and was synthesized by the base-catalyzed (NaOH, EMD) reaction of

phenol and formaldehyde (37 wt% in H_2O, Aldrich) following literature protocols.[18] Briefly in a typical preparation, 8 g of phenol was heated to 40-42°C to create a melt; subsequently, 1.7 g of 20 wt % NaOH aqueous solution was added dropwise under constant stirring. After 10 min, 14.16 g of formaldehyde (37 wt % in H_2O) was gradually added into the heated flask (< 50 °C). The condensation reaction was allowed to proceed under reflux at 75°C for 1 h and then cooled to ambient temperature. The pH was adjusted to approximately 7.0 by dropwise addition of 2 M HCl. The aqueous product was dried by rotary vacuum evaporation at 47-48 °C and then diluted in tetrahydrofuran (THF) to form 30 wt% resol solution with sodium chloride precipitate removed from the solution prior to its use. Polystyrene-b-poly(ethylene oxide) (PS-b-PEO) (M_n=44,300 g/mol, PDI=1.04, f_{PEO}=0.699) diblock copolymer was synthesized by anionic polymerization and used to template the mesoporous carbon films. To expand the pore size, homopolymer polystyrene (h-PS) (M_n=2170 g/mol, PDI=1.04) was used as pore-swelling agent and purchased from Varian Polymer Laboratories.

2.B.2 Synthesis of Large-Pore Mesoporous Carbon Film

Large pore mesoporous carbons with variable pore size were prepared using the evaporation induced self-assembly (EISA) method with h-PS as the pore swelling agent, PS-PEO as template, and resol as the carbon precursor, which were dissolved initially in THF to 6 wt % solids. The PS-b-PEO to resol weight ratio was 1.9:1. The amount of h-PS was varied from 0 to 20 wt % with a nomenclature of PS-PEO-PSx where x is the wt% of h-PS added to the template. The solutions were spin coated on clean silicon oxide wafers at 4000 rpm for 45s. The phenolic resin in the films was then crosslinked by heating to 120 °C for 24 h.

After thermopolymerization, the films were carbonized at 800°C for 3 h. Heating rate of 1°C min^{-1} was used for temperatures below 600°C and 5°C min^{-1} above 600°C.

2.B.3 Film Characterization

Film thickness and optical properties were determined using a variable angle spectroscopic ellipsometer (VASE M-2000, J.A. Woolam Co.) over the wavelength range from 250 - 1700 nm at incident angles of 65°, 70° and 75°. Ellipsometric porosimetry (EP)[29] was utilized for assessing the pore size distribution (PSD) by using toluene as the probe molecule to fill the pores via capillary condensation. Mass flow controllers (MKS) were used to change the flow rates of saturated toluene and compressed dry air streams to vary the partial pressure during the adsorption-desorption processes. From the adsorption isotherms, PSD were estimated through the application of the Kelvin equation. The Kelvin radius, r_k, was subsequently corrected for the thickness, t, of the adsorbed layer on the pore walls prior to capillary condensation, such that the pore radius is $r_p = r_k + t$. The thickness, t, was obtained as defined by Brunauer, Emmett and Teller (BET) methodology. The film porosity was quantified using the Bruggemann Effective Medium Approximation (BEMA) from the refractive indices of the neat film and after equilibration with saturated toluene vapor assuming that all pores were filled after toluene exposure and only two phases exist, amorphous carbon and voids. Surface topography of the carbonized films was characterized using an atomic force microscope (Park XE-150 AFM) in tapping mode. Cross-sectional micrographs of the carbonized films were obtained using transmission electron microscopy (TEM) (JEOL 2010F operating at 200 keV).

2.C. Results and Discussion

Ultra-large pore mesoporous carbon powders templated with poly(ethylene-oxide)-b-polystyrene diblock copolymers can be synthesized by pore swelling with homopolymer of polystyrene (*h*-PS).[24] However, there have been several reports of alteration of the phase behavior for the organic-organic self-assembled mesoporous carbon films.[20,21] As components can surface segregate in polymer blends,[30] this route might not be effective for either forming ordered mesoporous films or tuning the pore size. To initially assess the morphology of the synthesized films, ellipsometry is utilized. The ellipsometric angles ψ and Δ for carbonized film based on PS-PEO-PS20 are shown in Figure 2.1; these angles are fit using a generalized oscillator model based on Gaussian and Lorentzian functions to obtain the refractive index of the film as shown in Figure 2.1C. However to obtain a high quality fit, a uniform refractive index through the film cannot be utilized; instead a graded layer is needed with a significant increase in *n* near the free surface as illustrated in Figure 2.1D. The *n* at the surface is consistent with a dense amorphous carbon[31] and suggests that surface segregation might impact the morphology of these mesoporous carbons. Similar gradients in refractive index are observed for all the carbons templated by PS-PEO irrespective of the content of h-PS used to expand the pores.

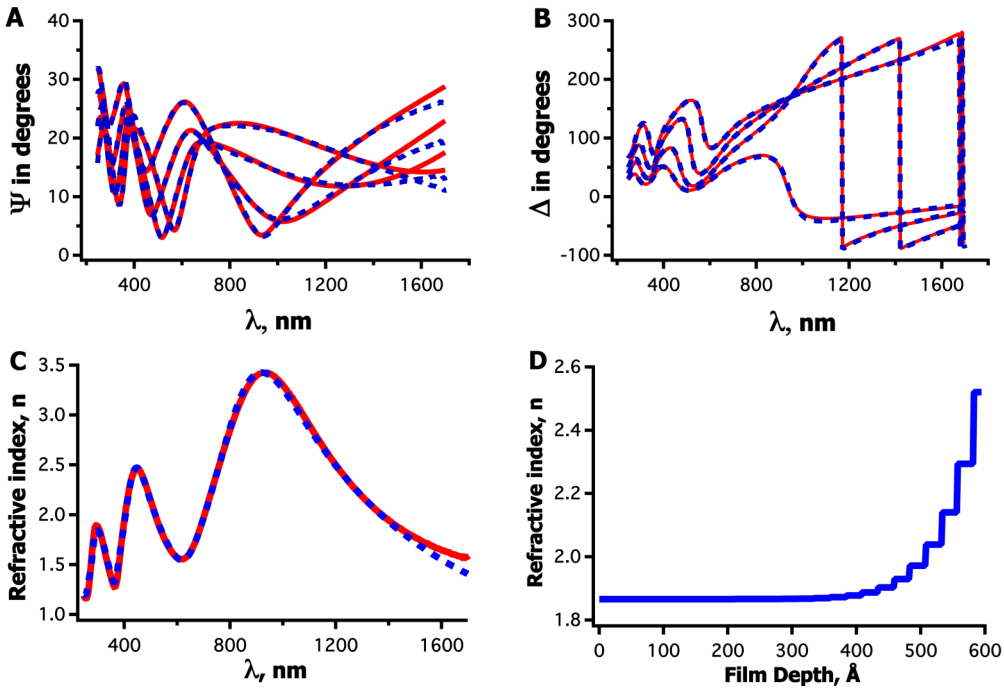

Figure 2.1. Measured ellipsometric angles (solid red lines) with the best fit (dashed blue lines) for (A) Ψ and (B) Δ for (PS-PEO)-PS20 film carbonized at 800°C with the refractive indices as a function of wavelength (C) and film thickness for λ=633 nm (D) as determined from the best fit.

To start to understand the impact of the added h-PS on the morphology and structure of these carbon films, the refractive index at λ=633 nm of the bulk film (e.g., thickness independent *n*, corresponding to <250 Å in Figure 2.1D) is examined as a function of h-PS loading as shown in Figure 2.2A. *n* is nearly independent of h-PS loading from PS-PEO-PS0 to PS-PEO-PS10 with a slight decrease from 1.926 to 1.912 (λ =632 nm) for these films respectively, but then significantly decreases for PS-PEO-PS20. As all films use the same carbon precursor and are carbonized at the same temperature, the refractive index of the wall material should be independent of h-PS loading; a decrease in *n* would indicate an increased porosity due to n_{air}=1. It is interesting that the refractive index is only slightly decreased at 10 wt % h-PS loading. For mesoporous carbon powders, this concentration of h-PS increases the pore volume from 0.71 cm^3/g to

0.97 cm^3/g, while the further increase to 20 wt % h-PS only increases the pore volume to 1.10 cm^3/g.[24] This suggests that the pores are initially not substantially swollen by the addition of h-PS for the thin films; however, the significant stresses that are imposed by carbonization due to interfacial pinning leads to essentially uniaxial contraction,[17] which could also impact the porosity of the film. Figure 2.2B illustrates how the film shrinkage during carbonization depends upon the homopolystyrene addition; contrary to reports for powders,[24] which found that adding h-PS actually decreases contraction during carbonization. To attempt to explain this contrasting behavior, the pore-swelling agent (h-PS) here is lower molecular mass (2.1 kg/mol) than in the previous case (5.1 kg/mol), but the PS segment of the copolymer is also smaller, so chain stretching argument for different h-PS distributions[32] is unlikely to explain the data. A shift in the symmetry of the copolymer phase in comparison to the bulk equilibrium phase due to the influence of the interfaces (substrate and air) has been observed for both pure block copolymer films[33] and mesoporous films.[34] Moreover, the bulk powders have been reported to exhibit a FCC geometry[24] instead of the more common BCC arrangement for diblock copolymers.[35] As the contraction of the films is directly related to the mechanics,[36] a change in the morphology between the thin film and bulk powder could potentially explain the differences in contraction of the mesostructure.

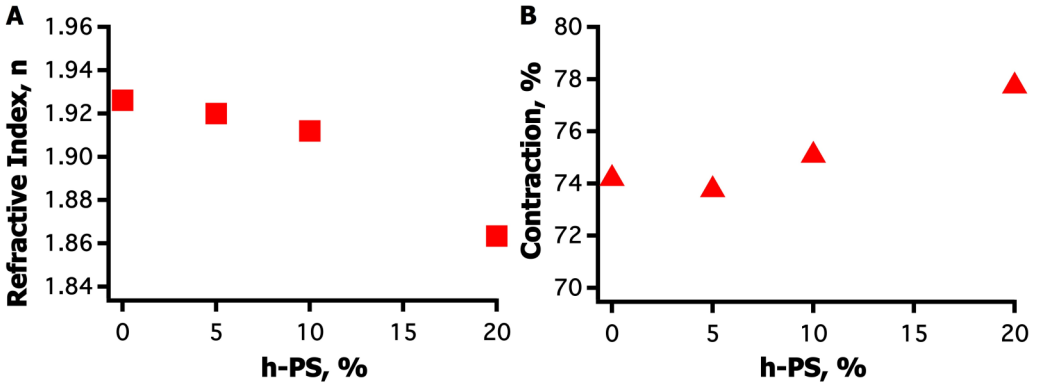

Figure 2.2 Impact of h-PS loading on the refractive index (λ= 633 nm) of the carbonized film and film contraction (B) during pyrolysis at 800 °C. All films are approximately 60 nm thick.

To further examine how the addition of h-PS impacts the structure of these films, the pore size distribution is estimated using ellipsometric porosimetry (EP),[29] where the sorption isotherms (Figure 2.3A) using toluene as the probe molecule are based upon the changes in refractive index that occurs during capillary condensation. A type-IV isotherm is observed for all the carbon films irrespective of the concentration of h-PS in the template. At low partial pressures, there is a modest increase in the refractive index as the micropores in the walls are filled with toluene. Then an increase in *n* from partial pressures of 0.7-0.9 occurs due to capillary condensation within the templated mesopores. For the desorption isotherm, there is an unusual multi-step profile with a fraction of the mesopores emptying at P/P_o ~ 0.8 and a second step at ~0.4-0.6 depending upon the h-PS fraction. Despite the relatively small differences in *n* and contraction (Figure 2.2) for h-PS loadings below 10 wt %, there is a shift in the adsorption isotherm to higher pressures for pore filling as the h-PS concentration is increased for the templated synthesis. This change in pore size can be estimated by application of the Kelvin equation with the pore size distributions (PSD) for the films illustrated in Figure 2.3B. Consistent with

templated synthesis, a relatively narrow size distribution is found when no h-PS is added with an average (mode) pore radius of 6.7 nm. By addition of 5 % h-PS to the template, the average pore size shifts to 6.9 nm with only a slight increase in the distribution of mesopores. This relative shift in the PSD is qualitatively consistent with previous results for powders,[24] but fractional increase in pore size is significantly different as the average pore size increases by 1.45 times for the powder, while there is a factor of 1.03 increase in pore size for the films examined here. This minimal increase in pore size is somewhat expected as the refractive indices of these films are very similar (Figure 2.2). Interestingly, the increase to 10 % h-PS significantly broadens the PSD, while increasing the average pore radius (8.8 nm). This change in the pore size distribution is significantly different from the analogous powders, which do not demonstrate any significant broadening of the PSD until > 20 wt % h-PS is added. From the change in refractive index between the unfilled (P/P_o =0) and filled ($P/P_o \approx 1$), the porosity of the films can be calculated assuming that all the pores are filled with toluene liquid. As shown in Figure 2.3C, the calculated porosity of the films is unchanged as the fraction of h-PS in the templating solution is increased up to 10 %. This result is consistent with the refractive indices determined from ellipsometry for these films (Figure 2.2). There is an increase in the porosity at 20 % h-PS in the template, which is also consistent with the refractive index of this film.

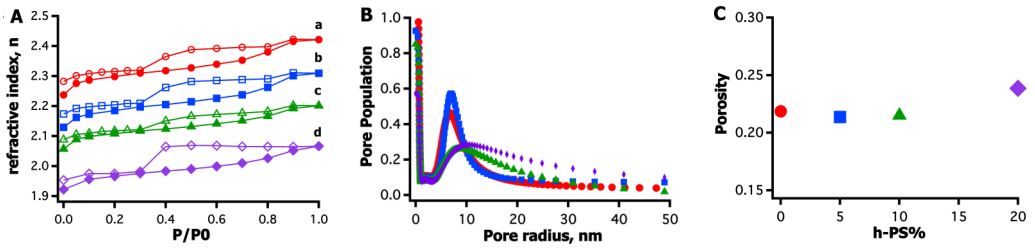

Figure 2.3. Toluene-vapor sorption isotherms (A) and corresponding pore size distributions (PSD, B) of PS-PEO-PS0 (●), PS-PEO-PS5 (■), PS-PEO-PS10 (▲), and PS-PEO-PS20 (◇) after carbonization at 800°C. The adsorption isotherms are shown with the closed symbols, while open symbols are the desorption isotherms. Isotherms a-c are offset by 0.3, 0.2, and 0.1, respectively. The pore size increases with addition of h-PS, but also appears to broaden the distribution. The film porosity (C) is relatively unchanged by the h-PS addition except for the highest loading examined.

To examine the structure of these films more carefully, AFM is utilized to characterize the surface morphology of the mesoporous carbon films as shown in Figure 2.4. Unlike most block copolymer films, the lateral ordering of these pores is rather poor. Moreover, we have previously shown good ordering of the surface of mesoporous carbons using the same resol precursor, but Pluronic surfactants as the template.[37] As T_g of PS is 105 °C, the hydrophobic domains in these samples during film formation can rapidly become glassy. Additionally, thermal annealing to improve the ordering will also act to crosslink the resol in the system, so the mobility of the PS domains to re-arrange into improved ordered structures is constrained by temperature; at low temperatures, the film is glassy and immobile, while at high temperatures, crosslinking of the resol occurs more rapidly than PS re-arrangement and locks the structure in place. Despite this challenge in ordering, it is remarkable that the PSD is narrow for the low concentrations of h-PS as determined from ellipsometric porosimetry (Figure 2.3). Similar to these data, the pore size of the mesopores on the surface appears to grow larger as h-PS is added. Additionally, the distribution of sizes observed

across the surface can be quantified via image analysis. These distributions as determined from multiple micrographs are illustrated in Figure 2.4. The mean pore radius shifts from 11 nm to approximately 14 nm as the h-PS loading increases from 0 % to 20 wt%. First, this fractional shift is comparable to that observed from the EP measurements. Moreover, the average pore radius on the surface is quantitatively significantly different; for example, the average pore radius from EP is only 6.7 nm, while the surface appears to have 11 nm or larger pores in general.

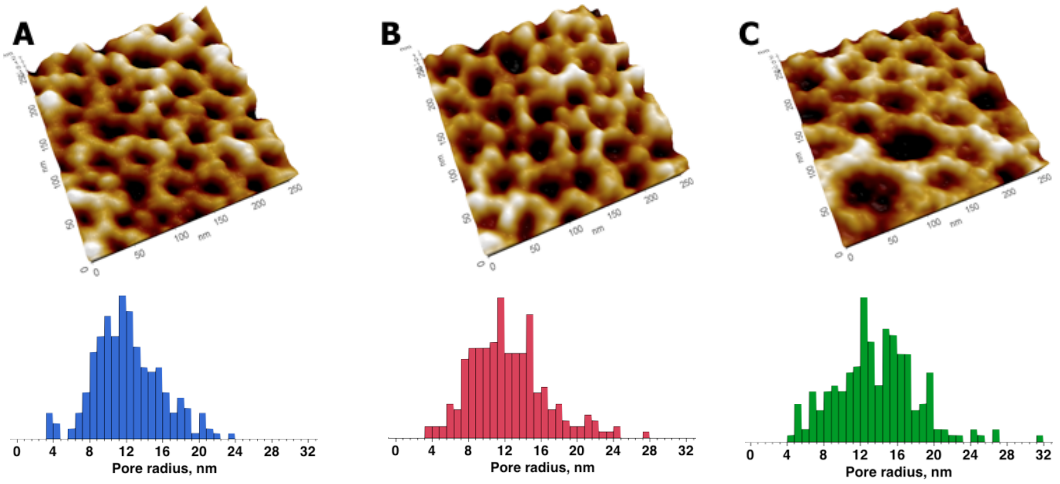

Figure 2.4. Surface topology and corresponding pore size distributions based on AFM micrographs for PS-PEO-PS0 (A), PS-PEO-PS10 (B), and PS-PEO-PS20 (C). The average pore size increases slightly and broadens (skewed towards larger sizes) as the h-PS is added.

To understand these differences, the carbonization process for the films must be taken into account. During carbonization, there is a significant loss of material that leads to shrinkage of the carbon mesostructure. For bulk powders, this contraction is isotropic; however for thin films, there is a constraint to shrinkage parallel to the substrate due to adhesion of the film to the very rigid silicon. This confinement leads to uniaxial contraction through the film thickness, which leads to anisotropic pores. Figure 2.4 illustrates the highly

anisotropic pores present in the mesoporous films. For the clear individual mesopores in the micrograph of the PS-PEO-PS20 carbonized film, the diameter of the pores in-plane is approximately 22.6 ± 3.4 nm; while through the plane of the film, the mesopores have a diameter of approximately 5.3 ± 0.6 nm. The ratio of these sizes for the pores is approximately 4; based upon the contraction of the films determined from ellipsometry, an aspect ratio in the range of 4:1 (in-plane:through-plane) would be expected for uniaxial contraction. Similar to the AFM micrographs of the surface, the cross section TEM micrographs (figure 2.5) also show the lack of long range order in these systems. It is clear that the films are highly porous with a common size amongst the pores, which is consistent with the PSD obtained from EP measurements. However, the space group for these mesopores is not clear from these images (or even if these are arranged on a common lattice).

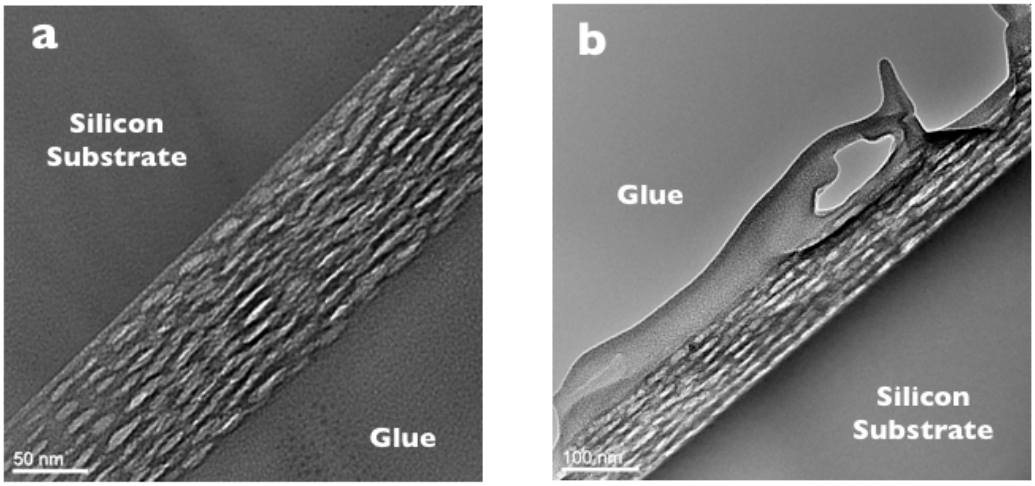

Figure 2.5. TEM cross section micrographs of (a) PS-PEO-PS0 and (b) PS-PEO-PS20.

GISAXS provides insight into the morphology of these templated films as illustrated in Figure 2.6; all films exhibit a similar scattering pattern irrespective

of the h-PS loading, both before (but after thermopolymerization) and after carbonization. There are clear diffraction peaks resulting from in-plane correlations, but only a single order is observed. Interestingly below the critical edge of the sample (Figure 2.6A), a powder ring can clearly be observed in the scattering, which indicates a loss in the orientation symmetry of the domains. As these films are relatively thin, it would be expected that the interfaces would direct the ordering of the block copolymer through the film thickness. For mesoporous carbon films that use organic-organic assembly of pluronic surfactants, excellent orientation through the plane of the film has been commonly observed.[19,37,38] In many cases, these films have been hundreds of nm thick, which would decrease the influence of the interfaces. For the PS-PEO block copolymer utilized here, the poor ordering would be consistent with the film being initially disordered or very poorly ordered, which is similar to spin coating of many block copolymers from good solvents,[33,39] but counter to the typically suspected EISA mechanism[40] for these mesoporous carbons.[41] For bulk powders, the slow evaporation of solvent may act to "solvent anneal"[23,42] the system into an ordered morphology. Moreover, diffusion limitation near a solid substrate in the thin films[43] may also act to depress the ordering kinetics relative to the bulk, which would also decrease the ordering extent. For the in-plane scattering from GISAXS, there is an interesting twinning of the primary reflection as more clearly shown in Figure 2.7.

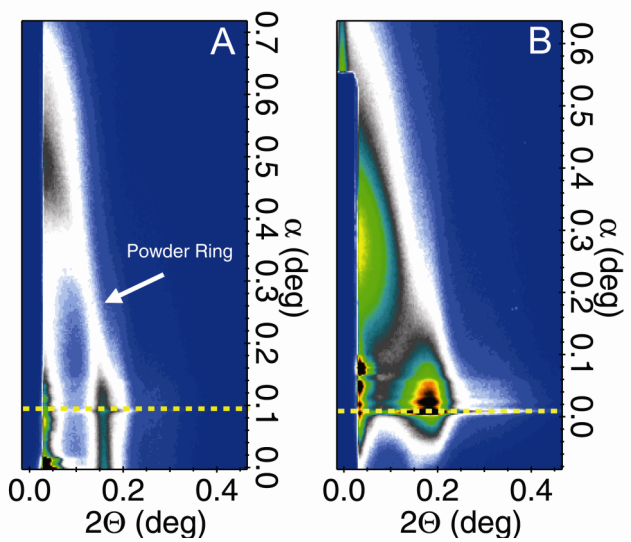

Figure 2.6. GISAXS profiles for carbonized PS-PEO-PS10 at incident angles of (A) 0.05° and (B) 0.30°, which is below and above the critical angle of the film, respectively.

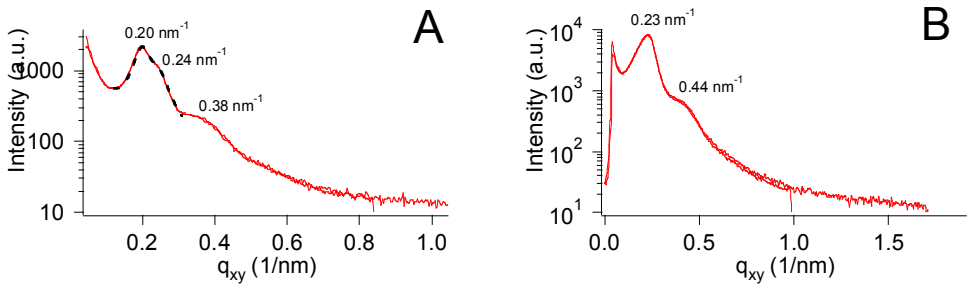

Figure 2.7. Line profiles of the in-plane scattering of PS-PEO-PS10 (as shown by the dashed line in the GISAXS data in Figure 2.6) for incident angles of (A) 0.05° and (B) 0.30°; the fit of the splitting of the primary peak is shown by the dashed line in part A.

Peak splitting is observed for incident angles below 0.20°, except for PS-PEO-PS20, where only a single peak can be resolved in the data (as illustrated in Figure 2.8). At these low angles, there is an increase in the d-spacing as more hPS is added to the template as would be expected for swelling of the hydrophobic domains of the template. These differences at low angles near the critical edge suggest a mixed 'morphology' or a surface wetting layer whose space group differs from the bulk. Interestingly, there is no statistical difference in the

d-spacing obtained at larger (≥ 0.20°) angles, irrespective of the hPS loaded into the template. This behavior is consistent with a change in the packing arrangement of the mesopores near the free surface that has previously been reported for pluronic templated mesoporous carbon films[21,37] and similar behavior has been seen in thin block copolymer films where a symmetry change is observed for thin films.[44] Due to the lack of higher order reflections, we cannot accurately assess the space groups present in these films; there is a second reflection at approximately 1.9q^* for most samples in the q_x plane, but q_z data are limited. However for the film with 20 % hPS added to the template, no splitting of the peaks is observable and the d-spacing remains statistically constant for all incident angles examined. One possible explanation for this behavior could be a thicker hPS wetting layer that changes the interfacial interactions during self assembly. This wetting layer would then be removed during the carbonization process; this hypothesis is consistent with the decrease in the relative ratio of the carbonized film thickness to the as-made thickness as the concentration of hPS in the template increases (see Figure 2.2B).

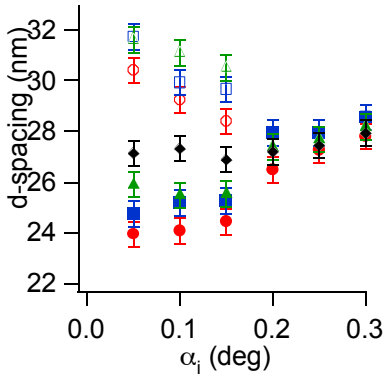

Figure 2.8. Splitting of primary peak in GISAXS profiles of carbonized mesoporous films for PS-PEO-PS0 (●), PS-PEO-PS5 (■), and PS-PEO-PS10 (▲) with larger d-spacing shown in open symbol at low incident angles. No splitting is observed for PS-PEO-PS20 (◇).

Moreover in examining the GISAXS profiles at multiple incident angles, the effective density of the films can also be assessed qualitatively as a function of depth. There is a tremendous shift in the apparent density of the film as the incident angle is varied; the density increases as the free surface is approached, which is estimated to be approaching 2 g/cm^3. This variation in physical density is consistent with the depth dependent refractive index determined from ellipsometry (Figure 2.1D). Overall, these results further illustrate the differences between thin films and bulk powders of soft templated, mesoporous carbons. Moreover, these data suggest that the formation of the self-assembled morphology does not occur during the rapid evaporation in thin film fabrication using spin coating, but rather appears to be driven by thermal annealing that occurs concurrently with crosslinking of the phenolic resin. By proper selection of the templating block copolymer and processing, it should be possible to develop mesoporous carbons with a variety of non-equilibrium morphologies and structures by exploiting differences in temperature dependencies of block copolymer self-assembly and phenolic resin crosslinking rates.

2.D. Conclusions

Soft templated mesoporous carbon films (ca. 60 nm thick) are fabricated by cooperative assembly of poly(styrene-block-ethylene oxide) (SEO) with phenolic resin with pore sizes tuned by the addition of polystyrene oligomers (hPS) to this self-assembling system. Unlike bulk powders where addition of hPS swells the hydrophobic domains leading to larger pores, the addition of hPS to the template in thin films does not significantly alter the film porosity or average pore size for less than 20 % hPS. From GISAXS analysis, the surface morphology appears to be different from the bulk of the film for hPS < 20 %; while for this

highest hPS loading, only a single structure appears to be present throughout the film. Both the surface morphology differences and lack of difference in the pore size with added hPS can be attributed to surface wetting of the oligomer. From TEM, squashed ellipsoid pores with a 4:1 ratio are found to be present throughout the films, fairly consistent with uniaxial contraction associated with the observed film contraction during carbonization. Both ellipsometry and GISAXS data analysis suggest densification of the films near the free surface. Moreover, the pores lack long range order as determined by TEM, AFM and GISAXS, which is counter to the well ordered mesopores observed when using even larger molecular mass block copolymer templates for the synthesis of bulk powders.[24] These data contradict the well held belief that the mesostructure of soft templated mesoporous carbons forms during solvent evaporation (EISA) and suggest that ordering is driven by thermal annealing that occurs concurrently with crosslinking of the phenolic resin.

2.E. References

1. Sanchez, C.; Boissiere, C.; Grosso, D.; Laberty, C.; Nicole, L. *Chemistry of Materials* **2008**, *20*, 682.

2. Schuth, F. *Chemistry of Materials* **2001**, *13*, 3184.

3. Barton, T. J.; Bull, L. M.; Klemperer, W. G.; Loy, D. A.; McEnaney, B.; Misono, M.; Monson, P. A.; Pez, G.; Scherer, G. W.; Vartuli, J. C.; Yaghi, O. M. *Chemistry of Materials* **1999**, *11*, 2633.

4. Zhuang, X.; Wan, Y.; Feng, C.; Shen, Y.; Zhao, D. *Chemistry of Materials* **2009**, *21*, 706.

5. Hudson, S.; Cooney, J.; Magner, E. *Angewandte Chemie-International Edition* **2008**, *47*, 8582.

6. Corma, A. *Chemical Reviews* **1997**, *97*, 2373.

7. Vinu, A.; Miyahara, M.; Ariga, K. *Journal of Physical Chemistry B* **2005**, *109*, 6436.

8. Beck, J. S.; Vartuli, J. C.; Roth, W. J.; Leonowicz, M. E.; Kresge, C. T.; Schmitt, K. D.; Chu, C. T. W.; Olson, D. H.; Sheppard, E. W.; McCullen, S. B.; Higgins, J. B.; Schlenker, J. L. *Journal of the American Chemical Society* **1992**, *114*, 10834.

9. Zhao, D. Y.; Feng, J. L.; Huo, Q. S.; Melosh, N.; Fredrickson, G. H.; Chmelka, B. F.; Stucky, G. D. *Science* **1998**, *279*, 548.

10. Holland, B. T.; Blanford, C. F.; Stein, A. *Science* **1998**, *281*, 538.

11. Brinker, C. J.; Dunphy, D. R. *Current Opinion in Colloid & Interface Science* **2006**, *11*, 126.

12. Stein, A. *Advanced Materials* **2003**, *15*, 763.

13. Ryoo, R.; Joo, S. H.; Jun, S. *Journal of Physical Chemistry B* **1999**, *103*, 7743.

14. Ryoo, R.; Joo, S. H.; Kruk, M.; Jaroniec, M. *Advanced Materials* **2001**, *13*, 677.

15. Liang, C. D.; Dai, S. *Journal of the American Chemical Society* **2006**, *128*, 5316.

16. Meng, Y.; Gu, D.; Zhang, F. Q.; Shi, Y. F.; Yang, H. F.; Li, Z.; Yu, C. Z.; Tu, B.; Zhao, D. Y. *Angewandte Chemie-International Edition* **2005**, *44*, 7053.

17. Tanaka, S.; Nishiyama, N.; Egashira, Y.; Ueyama, K. *Chemical Communications* **2005**, 2125.

18. Meng, Y.; Gu, D.; Zhang, F.; Shi, Y.; Cheng, L.; Feng, D.; Wu, Z.; Chen, Z.; Wan, Y.; Stein, A.; Zhao, D. *Chemistry of Materials* **2006**, *18*, 4447.

19. Schuster, J.; Koehn, R.; Keilbach, A.; Doeblinger, M.; Amenitsch, H.; Bein, T. *Chemistry of Materials* **2009**, *21*, 5754.

20. Song, L.; Feng, D.; Fredin, N. J.; Yager, K. G.; Jones, R. L.; Wu, Q.; Zhao, D.; Vogt, B. D. *Acs Nano* **2010**, *4*, 189.

21. Vogt, B. D.; Chavez, V. L.; Dai, M.; Arreola, M. R. C.; Song, L.; Feng, D.; Zhao, D.; Perera, G. M.; Stein, G. E. *Langmuir* **2011**, *27*, 5607.

22. Feng, D.; Lv, Y.; Wu, Z.; Dou, Y.; Han, L.; Sun, Z.; Xia, Y.; Zheng, G.; Zhao, D. *Journal of the American Chemical Society* **2011**, *133*, 15148.

23. Liang, C. D.; Hong, K. L.; Guiochon, G. A.; Mays, J. W.; Dai, S. *Angewandte Chemie-International Edition* **2004**, *43*, 5785.

24. Deng, Y.; Liu, J.; Liu, C.; Gu, D.; Sun, Z.; Wei, J.; Zhang, J.; Zhang, L.; Tu, B.; Zhao, D. *Chemistry of Materials* **2008**, *20*, 7281.

25. Kruk, M.; Cao, L. *Langmuir* **2007**, *23*, 7247.

26. Blin, J. L.; Otjacques, C.; Herrier, G.; Su, B. L. *Langmuir* **2000**, *16*, 4229.

27. Derylo-Marczewska, A.; Marczewski, A. W.; Skrzypek, I.; Pikus, S.; Kozak, M. *Applied Surface Science* **2008**, *255*, 2851.

28. Cao, L.; Man, T.; Kruk, M. *Chemistry of Materials* **2009**, *21*, 1144.

29. Baklanov, M. R.; Mogilnikov, K. P.; Polovinkin, V. G.; Dultsev, F. N. *Journal of Vacuum Science & Technology B* **2000**, *18*, 1385.

30. Dai, K. H.; Kramer, E. J.; Shull, K. R. *Macromolecules* **1992**, *25*, 220.

31. Smith, F. W. *Journal of Applied Physics* **1984**, *55*, 764.

32. Shull, K. R.; Winey, K. I. *Macromolecules* **1992**, *25*, 2637.

33. Segalman, R. A. *Materials Science & Engineering R-Reports* **2005**, *48*, 191.

34. Nicole, L.; Boissiere, C.; Grosso, D.; Quach, A.; Sanchez, C. *Journal of Materials Chemistry* **2005**, *15*, 3598.

35. Bates, F. S.; Fredrickson, G. H. *Physics Today* **1999**, *52*, 32.

36. Song, L.; Feng, D.; Lee, H.-J.; Wang, C.; Wu, Q.; Zhao, D.; Vogt, B. D. *Journal of Physical Chemistry C* **2010**, *114*, 9618

37. Song, L.; Feng, D.; Campbell, C. G.; Gu, D.; Forster, A. M.; Yager, K. G.; Fredin, N.; Lee, H.-J.; Jones, R. L.; Zhao, D.; Vogt, B. D. *Journal of Materials Chemistry* **2010**, *20*, 1691.

38. Tanaka, S.; Katayama, Y.; Tate, M. P.; Hillhouse, H. W.; Miyake, Y. *Journal of Materials Chemistry* **2007**, *17*, 3639.

39. Kim, G.; Libera, M. *Macromolecules* **1998**, *31*, 2569.

40. Brinker, C. J.; Lu, Y. F.; Sellinger, A.; Fan, H. Y. *Advanced Materials* **1999**, *11*, 579.

41. Wan, Y.; Shi, Y.; Zhao, D. *Chemistry of Materials* **2008**, *20*, 932.

42. Cavicchi, K. A.; Russell, T. P. *Macromolecules* **2007**, *40*, 1181.

43. Lin, E. K.; Kolb, R.; Satija, S. K.; Wu, W. L. *Macromolecules* **1999**, *32*, 3753.

44. Stein, G. E.; Cochran, E. W.; Katsov, K.; Fredrickson, G. H.; Kramer, E. J.; Li, X.; Wang, J. *Physical Review Letters* **2007**, *98*.

Chapter 3

INFLUENCE OF FILM MORPHOLOGY ON DRUG UPTAKE AND RELEASE

3.A. Introduction

The demand for new materials that meet the requirements in biomedical applications such as drug delivery systems (DDS) increases and thus development of viable vehicles is of broad interest and remains to be a great challenge. Several materials have been explored including inorganic silica[1-4], carbon materials [5-8], as well as polymeric matrix[9-10] for drug delivery. Part of the material selection process for controlled DDS is to incorporate fundamental requirements, such as biodegradability and biocompatibility [3, 6, 11], apart from the desirable characteristics like small particle size, possess high loading capacity, demonstrate prolonged circulation, and specifically accumulate in required pathological sites[2, 12-15].

In the recent years, mesoporous materials have been widely studied, especially mesoporous silica nanoparticles (MSNs), as carriers for drug delivery systems due to their large pore volume, high surface area, ease of functionalization, biodegradability, and generally low cytotoxicity [2-3, 16-18]. Aside from these material characteristics, particle sizes should also be carefully examined in designing material sets for DDS. MSNs with particle size less than 200nm can effectively interact with biomolecules on the cell surface or into cells by intracellular endocytosis and thus have been successfully investigated in anti-cancer drugs, protein and gene delivery vehicles [15]. Additionally, investigation on hemocompatibility of MCM-41 type MSNs with different particle sizes was reported by Zhao et al and showed that only small (100-200nm) MSNs are considered potentially safe candidates for intravascular drug delivery. Adsorption

of large SBA-15 type MSNs (ca. 600nm) induced a strong local membrane deformation resulting to spiculation of the red blood cells, internalization of the particles, and subsequent hemolysis[19]. For cancer therapeutics, MSNs aid in the aqueous solubility as these particles have large surface areas and porous interiors that can be utilized as reservoirs for hydrophobic drugs and be able to deliver into targeted organs or cells[1]. In a study conducted by Lu et al, a representative hydrophobic drug, campotothecin (CPT), is incorporated into the pores of fluorescent MSNs (FMSNs) and is delivered into a variety of human cancer cells to induce apoptosis. The nanoparticles were roughly 130nm in diameter with mean pore size of about 2nm while the CPT molecule is 1.3nm x 0.6nm which is small enough to fit in the FMSNs pores. CPT was reported to have remained inside the nanoparticles and released in the hydrophobic regions of the cell compartments to exert the apoptotic effect[1].

In contrast to mesoporous silicas, highly-ordered mesoporous carbons have relatively higher surface areas and pore volumes[20,21], which can facilitate large amount of drug loading [22]. Additionally reports have shown that cytotoxicity level of carbon materials is lower than that of its silica analogue[6, 22-25]. Thus, research on mesoporous carbons remains to be a growing trend. To name a few of the studies conducted in this field, a group headed by Lin successfully prepared CMK-1 type mesoporous carbon nanoparticles (MCNs), using MCM-48 type MSN as template, to serve as transmembrane delivery vehicle in human cervical cancer cells (HeLa). These monodisperse MCNs have an average particle size of 150nm and utilized for intracellular release of cell membrane fluorescence dye, Fura-2, inside HeLA[6]. Moreover, Gu and co-workers was able to synthesize uniform hydrophilic MCNs through combined hydrothermal synthesis and hard

templating for sustained release of CPT. These MCNs are less than 200nm in size and were effective drug carriers to inhibit growth of MCF-7 (human breast adenocarcinoma) cells after controlled release [5].

As most of the mesoporous carbon studies are related to nanoparticles, there is limited work done on films which provides a window of opportunity to explore this research area. A previously reported investigation by Suh et al showed a retarded release kinetics on mesoporous silica film, characterized to have vertically aligned accessible pores with 9nm diameter and 160nm thickness, for the evaluated Rhodamine dyes and Mitoxantrone drug. The mesoporous silica film is able to adsorb 0.67μg per cm^2 with longest corresponding release in a period of 150mins [26]. Here, we evaluated mesoporous carbon films synthesized via evaporation induced self-assembly (EISA) method using varied templates, Pluronic P123, Pluronic F127, and PS-b-PEO, to be able to modify the pore structure and pore size. The prepared films are named FDU-15, FDU-16, and large pore PS-PEO, wherein the former possess two-dimensional hexagonal geometry while the last two formed cubic mesostructures, as reported previously[27-29]. Apart from pore size and mesostructure, film thickness and hydrophobicity are also investigated. The aforementioned factors are evaluated to determine the drug loading capacity for Mitoxantrone dihydrochloride and its subsequent release behavior in phosphate buffered saline (PBS) solution. The said material characteristics are factors to be considered when defining sustained drug release from porous materials. Controllable pore size allows different size of molecules suitable for drug delivery while an ordered pore network allows fine control of the drug load and release kinetics. Moreover, hydrophobicity of the film can be varied through different carbonization temperatures; the

hydrophobicity is an important factor to take into account when designing DDS as this affects the interaction of the materials with the biomembrane and also allows control of the drug loading and release. We find that significantly more mitoxantrone can be loaded into mesoporous carbon films in comparison to the prior reports with mesoporous silica films; moreover, the release can be extended to nearly 2 weeks with carbons in comparison to 150 min from the mesoporous silica film[26].

3.B. Experimental Section

3.B.1 Materials

Two different amphiphilic triblock copolymers based upon poly(propylene oxide)-block-poly(ethylene oxide)-block-poly(propylene oxide), Pluronic F127 (M_w = 12 600 g/mol, PEO_{106}-PPO_{70}-PEO_{106}) and Pluronic P123 (M_w = 5800, PEO_{20}-PPO_{70}-PEO_{20}) were used to template nanoporous films. Pluronic F127 was utilized to template films with a cubic geometry of near spherical pores (named as FDU-16), while Pluronic P123 templated near hexagonal packed cylindrical pores (named as FDU-15)[28]. An alternative template based upon polystyrene-b-poly(ethylene oxide) (PS-b-PEO) (M_n=44,300 g/mol, PDI=1.04) was synthesized by anionic polymerization and provided larger mesopores in the templated films. For the carbonizable precursor, phenol and formaldehyde (37 wt% in H_2O, Aldrich) were polymerized by base-catalyzed (NaOH, EMD) condensation in ethanol solution to form resol as described by Zhao and coworkers. In a typical preparation, about 8 grams of phenol was melted in a flask at approximately 40-42°C with 1.7g of 20%w sodium hydroxide (NaOH) aqueous solution added dropwise while constantly stirring. After 10 minutes, 14.16g of formaldehyde (37%w in H_2O) was gradually added into the flask heated

below 50°C. Subsequently, mixture was stirred for an hour at 75°C with water reflux system and cooled down to room temperature. The pH was adjusted by dropwise addition of 2M of hydrochloric acid (HCl) until it reached to approximately 7.0. Water was displaced by rotary vacuum evaporation at 47-48°C. The final product was diluted in ethanol (EtOH) to form 30%w resol solution and was left overnight to let sodium chloride (NaCl) precipitate. The resulting top clear solution was transferred to a glass container and served as the batch of carbon precursor for all film samples used in the experiments. Ethanol (200 proof, Aldrich) was utilized for formulating the solutions for film formation.

A model drug, Mitoxantrone dihydrochloride (Sigma Aldrich), was utilized for examination of the efficacy of the mesopores for loading and release. The release medium was phosphate buffered saline (PBS) solution prepared by mixing equal amounts (v/v) of NaCl (14.0 mM), Na_2HPO_4 (10 mM), and KCl (2.7 mM) in deionized water with pH adjusted to 7.4 by adding 2 M HCl.

3.B.2 Mesoporous Carbon Film Synthesis

All mesoporous carbon films were fabricated by first spin coating a solution containing resol and the templating agent in ethanol onto a clean silicon wafers at 4000 rpm for 45 s. The films were aged in an oven at 120°C for 24 hours to thermopolymerize (crosslink) the phenolic resin. These films were then carbonized at 800°C for 3 h in a tubular furnace with inert N_2 atmosphere with simultaneous decomposition of the template. The heating rate was set to 1°C min^{1} for temperatures below 600°C and 5°C min^{-1} above 600°C. Three different morphologies of films were fabricated by these methods: FDU-16, FDU-15 and large pore SO. To fabricate FDU-16, the molar ratio of the phenol/formaldehyde/NaOH/F127 was 1:2:0.1:0.006. In a typical procedure, 1 g

of 30 wt% resol in ethanol solution was mixed with 0.15 g of Pluronic F127 and diluted with additional ethanol to solid concentrations of 10 wt%, 15 wt%, 20 wt% and 35 wt% to obtain different film thickness. To fabricate FDU-15, a molar ratio of phenol/formaldehyde/NaOH/P123 of 1:2:0.1:0.012 was utilized with similar dilutions in ethanol used to create the desired film thickness. To fabricate large pore PS-PEO, PS-b-PEO as template and resol as the carbon precursor were dissolved in ethanol at 60 °C. The PS-b-PEO to resol mass ratio is 1.9:1.

3.B.3 Mitoxantrone Drug Loading and Release Processes

To investigate the drug loading capacity of the films with different thicknesses, mesoporous carbon films (1cm x 1cm) were placed in a flat-bottomed 24 well cell culture plate (Corning Costar) and were immersed in Mitoxantrone dihydrochloride solution (750uL, 0.02mM). The prepared samples were placed inside an incubation shaker (150 rpm) for 24 hours at 28°C. To quantify the amount of drug adsorbed on the films, absorbance of an aliquot of the Mitoxantrone dihydrochloride solution after adsorption by the mesoporous carbon film was measured using a spectrophotometer (Biotek Synergy 2). Drug-loaded films were dried at ambient conditions prior the release studies. For the release kinetics, films were placed in cuvettes with 3 mL of PBS solution and enclosed in vials which were immersed in a water bath with a 37°C temperature at constant stirring. Absorbance of the solution was collected at regular time intervals using UV-Visible spectrophotometer (Agilent 8453) to elucidate the release. Drug uptake and release amounts are calculated based upon the calibration curves from the standardized solutions.

3.B.4 Film Characterization

Film thickness and optical properties of the synthesized samples were determined by a variable angle spectroscopic ellipsometer (VASE M-2000, J.A. Woolam Co.) in the UV-vis-NIR wavelength range (250 - 1700 nm) using incident angles 65°, 70°, and 75°. Optical properties of as-made and carbonized films were estimated using a Cauchy model and a Lorentz-Lorentz-consistent general oscillator model, respectively. Moreover, ellipsometric porosimetry [31] was employed to assess pore size distribution (PSD) by utilizing toluene (Aldrich) as the probe molecule; the refractive index is monitored as a function of partial pressure with increases occurring due to capillary condensation of toluene in the pores. The partial pressure was controlled using relative flow rates of saturated toluene and compressed dry air streams by mass flow controllers (MKS).. From these sorption isotherms, the PSD was calculated by the application of the Kelvin equation. The Kelvin radius, r_k, was corrected for the thickness, t, of the adsorbed layer on the pore walls prior to capillary condensation, such that the pore radius is $r_p = r_k + t$. The thickness, t, was defined by the BET equation based upon the adsorption of the same adsorptive on a nonporous sample[31]. Aside from PSD, film porosity was quantified based upon the change in refractive index during the filling/emptying of the pores when the relative partial pressures reached unity. Assuming only two phases exist, amorphous carbon and voids, Bruggemann Effective Medium Approximation (BEMA) was applied to estimate the film porosity from the refractive indices. To characterize the morphology of the synthesized films, x-ray diffraction (XRD) was performed in a $\theta/2\theta$ geometry using Cu Kα (λ=1.542Å) source (Panalytical X'Pert PRO) with angle of incidence, 2θ, varied from 0.5 to 3.0°. A parallel plate collimator (PPC) was used in

combination with an incident beam optical module to provide an X-ray beam with a low fixed divergence. Surface topography of the carbonized films was characterized using an atomic force microscope (Park XE-150 AFM) in tapping mode. Cross-sectional micrographs of the carbonized films were obtained using transmission electron microscopy (TEM) (JEOL 2010F operating at 200 keV).

3.C. Results and Discussion

3.C.1 Effect of Pore Structure and Pore Size

3.C.1.1 Morphology of Synthesized Mesoporous Carbon Films

Highly-ordered mesoporous carbons are synthesized using soft supramolecular self-assembly through EISA method. Carbon films are synthesized with varying morphological characteristics, pore size and pore structure, to determine and evaluate its performance for drug uptake and release. As previously reported, FDU-15-800 films form a 2D hexagonal structure[27,28] while FDU-16-800[27,28] and PS-PEO-800 follows a cubic configuration. In order to understand the structure and morphology, a variety of different metrology tools are utilized to elucidate specifics of the morphology and pore size. Figure 3.1 illustrates the adsorption and desorption isotherms obtained using ellipsometric porosimetry (EP) for these carbon films. For FDU-15-800, the toluene-vapor isotherms exhibit an abrupt increase in refractive index at low partial pressure (P/P_o=0.05) with only a gradual increase in refractive index for any further increase in P/P_o. Application of the Kelvin equation to the adsorption isotherm provides an estimate of the mean pore size of FDU-15-800 films to be approximately 1.4 nm. During carbonization, the framework contracts and thus the pore size decreases in comparison to FDU-15 film with similar molar ratio of 0.012 processed at 350°C with a mean pore size of 3 nm[27]. The desorption

isotherm shows a small hysteresis loop, but the refractive index does not return to its original neat value even after flowing clean N2 over the sample for hours. This is consistent with the activated desorption previously reported by Song et al. for toluene desorption from carbonized FDU-16-800.

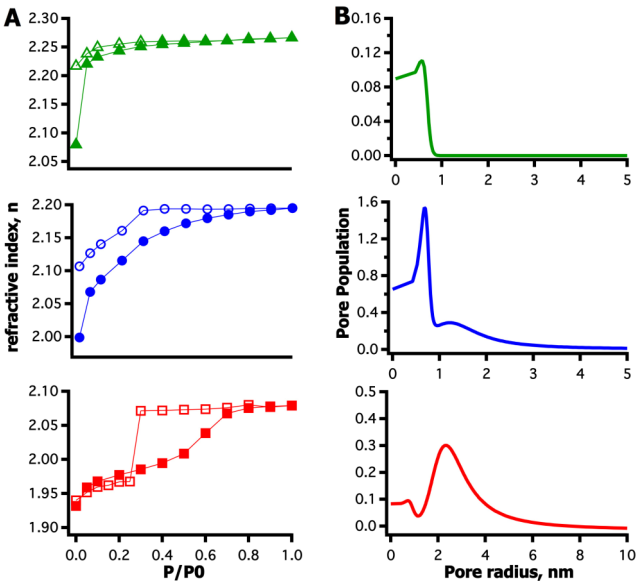

Figure 3.1. Toluene-vapor sorption isotherms (A) and corresponding pore size distributions (PSD, B) of FDU15-800 (▲), FDU16-800 (●), PS-PEO-800 (■) after carbonization at 800°C. The adsorption isotherms are shown with the closed symbols, while open symbols are the desorption isotherms. Refractive indices were determined at λ=633nm.

FDU-16-800, on the other hand, also showed an initially sudden increase in refractive index then a gradual change as the partial pressure is increased though it manifest a different profile which suggest a relatively larger pore size compared to that of FDU15-800. Mean pore size is about 2nm based from the PSD data. Mesoporous carbon PS-PEO-800 film possess larger pores based on the isotherms as the adsorption curve gradually increases then exhibit a significant change in refractive index *n* from partial pressures 0.5-0.8. The desorption isotherm displays a sudden drop as the toluene-vapor pressure is

decreased during the emptying of the pores at partial pressure P/P_o=0.3. Additionally, the change in refractive indices prior adsorption and at the point when the pores are filled can be used to determine film porosity using BEMA. This is estimated to be 18%, 21%, and 17% for FDU-15-800, FDU-16-800, and PS-PEO-800, respectively.

To further investigate on the structure of the films, XRD was used to determine if the synthesized films are ordered. The interplanar spacing, as shown in figure 3.2, suggest that PS-PEO-800 film has significantly large pore size compared to FDU-15-800 and FDU-16-800 which is congruent to the EP data. This is consistent with previously reported studies[27,28]. In addition, TEM images (figure 3.3) also exhibited similar results which strongly proves the correlation between EP and XRD data.

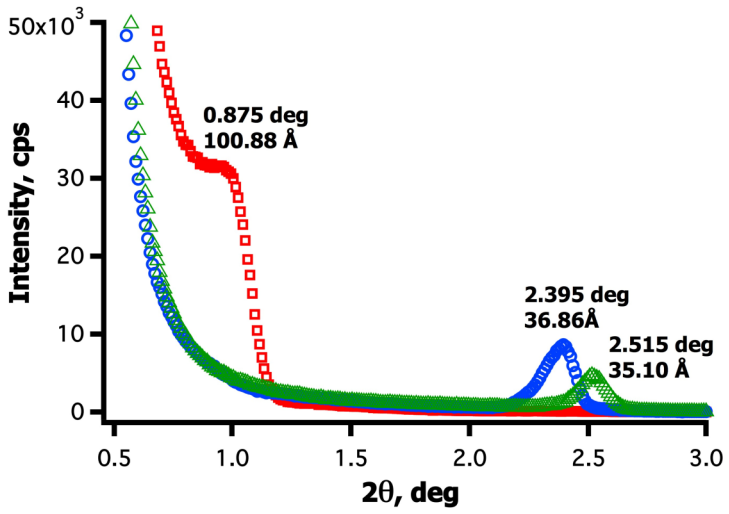

Figure 3.2. XRD profiles of the mesoporous carbon films FDU15-800 (△), FDU16-800 (○), PS-PEO-800 (□) after pyrolysis at 800°C.

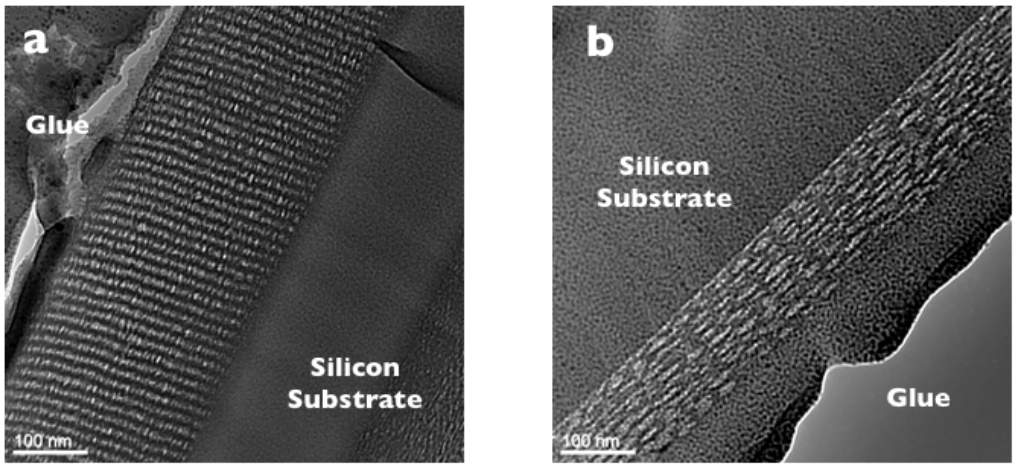

Figure 3.3. TEM images of (a) FDU16-20% and (b) PS-PEO carbonized at 800°C with corresponding film thickness of approximately 120nm and 80nm, respectively. Data showed that pores of PS-PEO-800 film are apparently larger than that of the FDU-16.

Surface topology of the PS-PEO-800 film is characterized with AFM, as shown in figure 3.4, and manifested large accessible pores at the surface with a mean pore radius of approximately 12.4nm. This is relatively larger compared to the data gathered from EP. The differences can be elucidated based on the mechanical constraints of the film to the silicon substrate as it experiences uniaxial contraction [27] during the carbonization process.

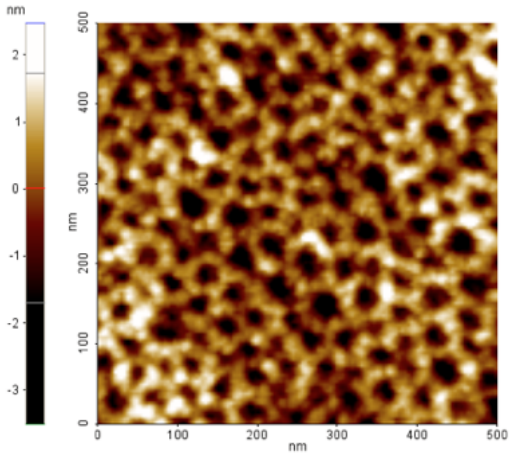

Figure 3.4. AFM micrograph of PS-PEO-800 film with a scan size of 500nm by 500nm and amplitude of 1.63μm.

3.C.1.2 Drug Uptake on Mesoporous Carbon Films

All the mesoporous carbon films are subjected to similar drug loading conditions at ambient temperature and initial concentration of Mitoxantrone dihydrochloride solution (0.02mM, 750μL). Uptake results showed that FDU-16-800 capacity is independent of the film thickness as it shows an approximately 2.62μg/cm² drug adsorbed across the samples evaluated. This behavior may suggest that adsorption is limited on the film surface and is unable to fill up the entire length of the pores. It is also possible that some of the mesostructures near the silicon substrate surface may have experienced pore shrinkage as opposed to the near surface post carbonization process. Interestingly, FDU-15-800 show higher adsorption at thicker films, 100nm and above, but a declining trend as it goes thinner than 100nm. Compared to FDU-16-800 films, its accessibility is limited as the cylindrical pores are oriented parallel to the silicon substrate. However, the length of the cylinders could have contributed to its drug loading capacity. The PS-PEO-800 films manifest high adsorption, at about 3.5μg/cm², primarily due to the presence of large pores which can accommodate more material within the mesostructural domains.

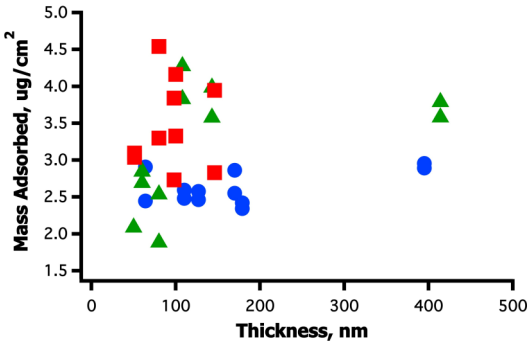

Figure 3.5. Mitoxantrone dihydrochloride drug loading capacity for FDU15-800 (▲), FDU16-800 (●), PS-PEO-800 (■) evaluated at different thicknesses after a 24-hour incubation at 28°C. Initial drug concentration is 0.02mM of 750μL solution.

3.C.1.3 Release Behavior in PBS solution

Figure 3.6 illustrates the release of the adsorbed Mitoxantrone dihydrochloride from the mesoporous carbon films in PBS solution at 37°C. The FDU-16-800 film manifest the highest amount of drug released at approximately 56% after 15-days. Interestingly, the released amount is significantly higher compared to FDU-15-800 and PS-PEO-800 even if the drug loaded is smaller relative to the latter carbon films. Almost similar behavior is observed for FDU15-800 and PS-PEO-800 with amount of release to be about 30%.

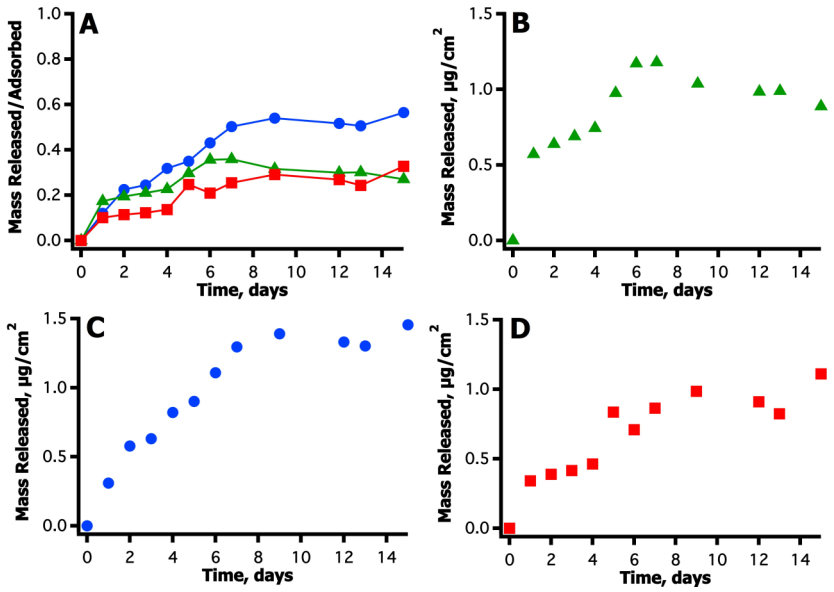

Figure 3.6. Profiles of FDU15-800 (▲), FDU16-800 (●), PS-PEO-800 (■) shown in % released (A) and corresponding mass release per area for corresponding films (B-D). Drug release was done at 37°C using a phosphate buffered saline (PBS) as release medium with pH=7.4.

A corresponding release amount per area is depicted on figure 3.6(B-D) which consistently showed a higher amount of drug is released from the FDU-16-800 film and relatively similar for FDU-15-800 and PS-PEO-800. An abrupt release is observed on all carbon films and gradually increases thereafter. Notice that FDU-16-800 have an increasing trend and gradually subsides after seven

days. It can be deduced that during this time, the solution has reached saturation. Even if the films are unable to reach an ideally 100% drug release, the sustained release profile is notably remarkable.

Compared to FDU16-800, the FDU15-800 film is somewhat expected to have slower desorption rate and lesser amount of drug released due to less accessible pores and smaller pore size. What seems unclear, is the release profile exhibited by the large-pore PS-PEO-800 films as some studies have proven otherwise [16,32]. Large pore size mesoporous materials tend to have an increased capacity for adsorption due to large internal surface area and similarly should have higher release primarily because of higher accessibility. Unless this behavior is similar to a previous study by Gultepe et al, wherein the kinetics of a sustained release is described by an activated surface-density-dependent desorption model[30]. Experiments conducted on anodic aluminum oxide with pore sizes 20nm and 200nm revealed 30% and 20% release of Doxorubicin, respectively, after 15 days. This behavior is further explained that the release profile follows density-activated release model wherein faster release rate is manifested when fewer number of drug molecules are left on the surface. Hence, the sustained release is determined not solely by the drug-surface interactions but also by the interaction between drug molecules.

3.C.2 Impact of Carbonization Temperature on Release

3.C.2.1 Morphology at Varying Carbonization Temperatures

The carbonization conditions play an important role in determining the properties of the mesoporous carbon materials. MCs prepared at low heating ramp rate (1°C/min) generate well ordered structures as these are virtually micropore free and exhibit only framework-confined mesoporosity. On the other

hand, fast heating ramp rate generates carbons with significant microporosity and some non-framework porosity[32]. Prepared films for this study are all subjected to a low heating ramp rate (1°C/min) below 600°C and is increased to 5°C/min above 600°C in a nitrogen environment. Nomenclature for the carbonized films is FDU-16-x where x denotes the temperature used during the carbonization process.

Figure 3.7 illustrates the adsorption-desorption isotherms based on refractive index changes for FDU-16-600, FDU16-800, and FDU-16-1000 after pyrolysis. The corresponding pore size distribution showed increasing number of micropores at increasing carbonization temperature which is in agreement with studies reported on mesoporous films[28]. Pore sizes also get smaller at higher temperatures.

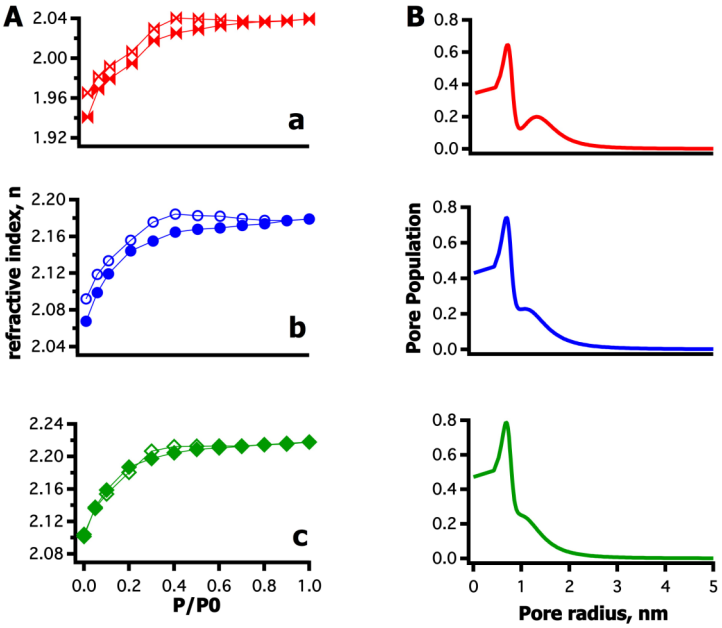

Figure 3.7. Ellipsometric data of (A) toluene-vapor isotherms for mesoporous carbon FDU-16 films pyrolyzed at 600°C (a), 800°C (b) and 1000°C (c). Refractive index decreases with increasing carbonization temperature while corresponding (B) PSD data show smaller pore sizes as temperature is increased.

To determine structural differences between films carbonized at different temperatures, XRD analysis has been employed. Interplanar spacing shifts (see figure 3.8) as temperatures increase which is in agreement with the mesostructural shrinkage during high thermal treatment. Initially, d-spacing is about 11.4nm after thermopolymerization and tends to decrease from 4.4nm, 3.7nm, to 3.4nm as thermally heated to 600°C, 800°C, and 1000°C, respectively. The corresponding contraction is estimated to be 61%, 68%, and 70%.

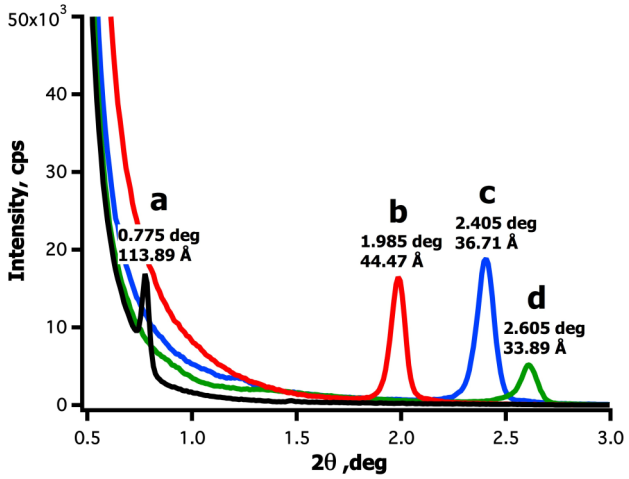

Figure 3.8. XRD profiles of mesoporous carbon FDU-16 films (a) as-made and pyrolyzed at (b) 600°C, (c) 800°C and (d) 1000°C. D-spacing shifts as thermal conditions increase congruent to contraction at higher temperatures.

Raman spectra (figure 3.9) for the different mesoporous carbon FDU16 films have distinct peaks at ~1580cm^{-1} (G-band) and ~1350cm^{-1} (D-band). The so-called G-line is a characteristic feature of the graphitic layers and corresponds to the tangential vibration of the carbon atoms. The existence of a G-band in all Raman spectra suggests that well-defined graphitic domains are indeed developed. The second characteristic mode is a typical sign for defective graphitic structures (D-line). The comparison of the ratios of these two peaks intensities gives a good indicator of the quality of the bulk samples. If these both bands have

similar intensity this indicates a high quantity of structural defects[33] which is observed on films carbonized at 800°C and 1000°C.

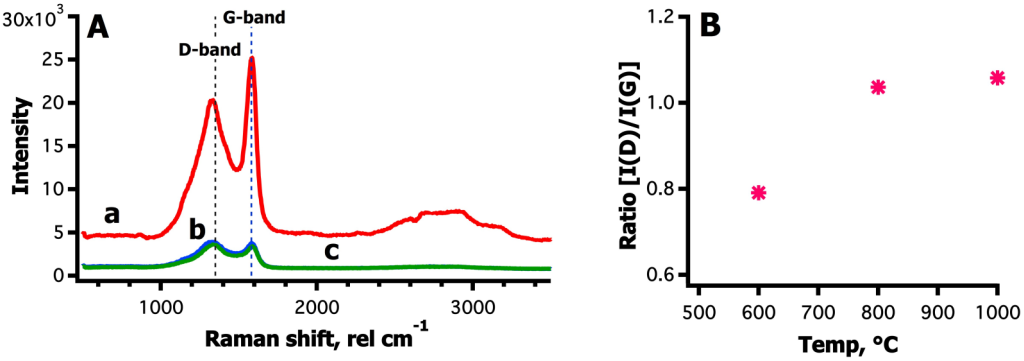

Figure 3.9. Spectra of D and G Raman bands (A) identified for FDU16 films pyrolyzed at temperatures (a) 600°C, (b) 800°C and (c) 1000°C using a 532nm excitation laser. Ratio of the D-band and G-band peaks intensities increase at increasing carbonization temperatures as shown in B.

3.C.2.2 Drug Uptake and Release of Carbonized Films

For the drug adsorption capacity (figure 3.10A), no significant difference is observed among materials even if carbonization temperatures are varied. However, these materials manifest different release behavior, as shown in figure 3.10B, with a declining trend as the carbonization temperature is increased. This profile is somewhat expected since the surface becomes more hydrophobic at increasing carbonization temperature and thus also increase the affinity of the less water-soluble Mitoxantrone drug resulting to less drug desorbing from the film surface. Additionally, the Raman data suggested a distinctly different bulk structure for the FDU-16-600 compared to the other two films which can contribute to the observed release performance.

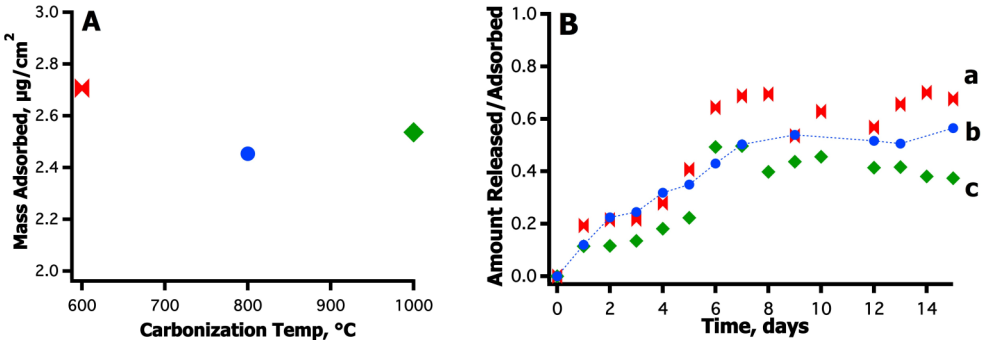

Figure 3.10. Loading (A) and release (B) profiles for FDU16 films carbonized at 600°C (a), 800°C (b), and 1000°C (c) at a temperature maintained at 37°C in a PBS release medium with pH=7.4.

3.D. Conclusions

Mesoporous carbon films are synthesized via evaporation induced self-assembly (EISA) method using phenolic resin and varied templates, Pluronic P123, Pluronic F127, and PS-b-PEO, to be able to modify the pore structure and pore size. The aforementioned factors are evaluated to determine the drug loading capacity for Mitoxantrone dihydrochloride and its subsequent release behavior in phosphate buffered saline (PBS) solution. The synthesized FDU-15, film possesses two-dimensional hexagonal geometry while FDU-16 and large pore PS-PEO films formed cubic mesostructures with pore sizes . Among the materials evaluated, FDU-16-800 exhibit the highest amount of drug desorbed (56%) compared to FDU-15-800 and PS-PEO-800 which similarly display an almost 30% release. The FDU-16-800 drug uptake is about 2.62µg/cm² with a subsequent controlled release monitored for 15 days and deemed to be thickness-independent which could suggest adsorption occurred beneath the surface. Interestingly, there is a larger capacity for FDU-15-800 and PS-PEO-800 which can be attributed to its morphological properties. FDU-15 have long cylindrical pores parallel to the silicon substrate while PS-PEO-800 possess large pores which have large internal surface area to accommodate more drug molecules.

However, this did not directly translate to a higher amount of drug release. This somewhat expected for FDU-15-800 film since it has relatively smaller pore size and less accessible pores due to its geometry. However, it is unclear on why PS-PEO-800 behaved differently compared to previous studies related to release of large pore size materials. It is hypothesized that aside from drug-surface interaction, the interaction between drug molecules could have an effect on its release behavior. In addition to pore size and pore structure, effect of film hydrophobicity to drug release is also investigated. Varying the film carbonization temperature changes hydrophobicity and this apparently provided an insight on release performance. Slower release is observed at increasing carbonization temperature. It is suggested that additional studies be done to further the understanding of the said results.

3.E. References

1. Lu, J., Liong, M., Zink, J. and Tamanoi, F. Mesoporous Silica Nanoparticles as a Delivery System for Hydrophobic Anticancer Drugs. *Small* **2007**, 3, 1341–1346.

2. Wu, S., Hung, Y. and Mou, C. Mesoporous silica nanoparticles as nanocarriers *Chemical Communications* **2011**, 47, 9972–9985.

3. Trewyn, B., Giri, S., Slowing, I., Lin, V. Mesoporous silica nanoparticle based controlled release, drug delivery, and biosensor systems *Chemical Communications* **2007**, 3236–3245

4. Suh, M., Lee, H., Park, J. Lee, U., Kwon, Y., Kim, D. A Mesoporous Silica Thin Film as Uptake Host for Guest Molecules with Retarded Release Kinetics *ChemPhysChem* **2008**, 9, 1402–1408.

5. Gu, J. Su, S. Li, Y., He, Q., Shi, J., Hydrophilic mesoporous carbon nanoparticles as carriers for sustained release of hydrophobic anti-cancer drugs *Chemical Communications* **2011**, 47, 2101-2103

6. Kim, T., Chung, P., Slowing, I., Tsunoda, M., Yeung, E., Lin, V. Structurally Ordered Mesoporous Carbon Nanoparticles as Transmembrane Delivery Vehicle in Human Cancer Cells *Nano Letters* **2008**, 8 (11), 3724–3727.

7. Zhu, S., Chen, C., Chen, Z., Liu, X., Li, Y., Shi, Y., Zhang, D. Thermo-responsive polymer-functionalized mesoporous carbon for controlled drug release *Materials Chemistry and Physics* **2011**, 126 (1-2), 357-363.

8. Wang, X., Liu, P., Tian, Y. Ordered mesoporous carbons for ibuprofen drug loading and release behavior *Microporous and Mesoporous Materials* **2011**, 142, 334–340

9. Oh, J-K., Drumright, R., Siegwart, D., Matyjaszewski, K. The development of microgels/nanogels for drug delivery applications *Prog. Polym. Sci.* **2008**, 33, 448–477.

10. Sokolsky-Papkov, M., Agashi, K., Olaye, A., Shakesheff, K., Domb, A. Polymer carriers for drug delivery in tissue engineering *Adv. Drug Deliv. Rev.* **2007**, 59, 187–206.

11. Watanabe, J. Iwamoto, S., Ichikawa, S. Entrapment of some compounds into biocompatible nano-sized particles and their releasing properties *Colloids and Surfaces B-Biointerfaces* **2005**, 42, 141–146.

12. Paolino, Donatella, et.al., *Drug Delivery Systems*. Encyclopedia of Medical Devices and Instrumentation, Second Edition, **2006** John Wiley & Sons, Inc.

13. Torchilin VP. Targeted Pharmaceutical Nanocarriers for Cancer Therapy and Imaging *AAPS Journal* **2007**, 9(2), Article 15.

14. Cho, K., Wang, X., Nie, S., Chen, Z., Shin, D. Therapeutic Nanoparticles for Drug Delivery in Cancer *Clin Cancer Res* **2008**, 14, 1310-1316.

15. Jin, S., Ye, K., Nanoparticle-Mediated Drug Delivery and Gene Therapy *Biotechnol. Prog* **2007**, 23, 32–41

16. S. Wang Ordered mesoporous materials for drug delivery *Microporous and Mesoporous Materials* **2009**, 117, 1–9.

17. Tsai, C.-P.; Chen, C.-Y.; Hung, Y.; Chang, F.-H.; Mou, C.-Y. Monoclonal Antibody-Functionalized Mesoporous Silica Nanoparticles (MSN) for Selective Targeting Breast Cancer Cells. *J. Mater. Chem.* **2009**, 19, 5737–5743.

18. Cheng, S.-H.; Lee, C.-H.; Chen, M.-C.; Souris, J. S.; Tseng, F.- G.; Yang, C.-S.; Mou, C.-Y.; Chen, C.-T.; Lo, L.-W. Tri-Functionalization of Mesoporous Silica Nanoparticles for Comprehensive Cancer Theranostics-the Trio of Imaging, Targeting and Therapy. *J. Mater. Chem.* **2010**, 20.

19. Zhao, Y., Sun, X., Zhang, G., Trewyn, B., Slowing, I., Lin, V. Interaction of Mesoporous Silica Nanoparticles with Human Blood Cell Membrane: Size and Surface Effects *ACS Nano* **2011**, 5 (2), 1366–1375.

20. Ryong, R., Joo, S., Jun, S. Synthesis of Highly Ordered Carbon Molecular Sieves via Template-Mediated Structural Transformation *The Journal of Physical Chemistry B* **1999**, 103 (37), 7743-7746.

21. R. Lu, Y. Shi, Y. Wan, Y. Weng, F. Zhang, D. Gu, Z. Chen, B. Tu. D. Zhao, Triconstituent Co-assembly to Ordered Mesostructured Polymer-Silica and Carbon-Silica Nanocomposites and Large-Pore Mesoporous Carbons with High Surface Areas *J. Am. Chem. Soc.* **2006**, 128, 11652-11662.

22. Fang, Y., Gu, D., Zou, Y., Wu, Z., Li, F., Che, R., Deng, Y., Tu, B. and Zhao, D., A Low-Concentration Hydrothermal Synthesis of Biocompatible Ordered Mesoporous Carbon Nanospheres with Tunable and Uniform Size. *Angewandte Chemie International Edition* **2010**, 49: 7987–7991.

23. Yan, A., Lau, B., Weissman, B., Külaots, I., Yang, N., Kane, A. and Hurt, R., Biocompatible, Hydrophilic, Supramolecular Carbon Nanoparticles for Cell Delivery. *Advanced Materials* **2006**, 18: 2373–2378.

24. Xu, Z. P.; Zeng, Q. H.; Lu, G. Q.; Yu, A. B. Inorganic nanoparticles as carriers for efficient cellular delivery *Chem. Eng. Sci.* **2006**, 61 (3), 1027–1040.

25. Yu, T., Malugin, A., Ghandehar, H. Impact of Silica Nanoparticle Design on Cellular Toxicity and Hemolytic Activity *ACS Nano* **2011**, 5 (7), 5717–5728

26. Suh, M., Lee, H., Park, J., Lee, U., Kwon, Y., Kim, D.. A Mesoporous Silica Thin Film as Uptake Host for Guest Molecules with Retarded Release Kinetics *ChemPhysChem* **2008**, 9, 1402 – 1408.

27. Song, L., Feng, D., Fredin, N., Yager, K., Jones, R., Wu, Q., Zhao, D., Vogt, B.. Challenges in Fabrication of Mesoporous Carbon Films with Ordered Cylindrical Pores via Phenolic Oligomer Self- Assembly with Triblock Copolymers *ACSNano* **2010**, 4, 189–198

28. Meng, Y., Gu, D., Zhang, F., Shi, Y., Cheng, L., Feng, D., Wu, Z., Chen, Z., Wan, Y., Stein, A., Zhao, D. A Family of Highly Ordered Mesoporous Polymer Resin and Carbon Structures from Organic-Organic Self-Assembly *Chem. Mater.* **2006**, 18, 4447-4464

29. Deng, Y., Yu, T., Wan, Y., Shi, Y., Meng, Y., Gu, D., Zhang, L., Huang, Y., Liu, C., Wu, X., Zhao, D. Ordered Mesoporous Silicas and Carbons with Large Accessible Pores Templated from Amphiphilic Diblock Copolymer Poly(ethylene oxide)-b-polystyrene *J. Am. Chem. Soc.* **2007**, 129, 1690-1697

30. Gultepe E, Nagesha D, Casse BD, Banyal R, Fitchorov T, Karma A, Amiji M, Sridhar S. Sustained Drug Release from Non-eroding Nanoporous Templates *Small* **2010**, 6, 213-216.

31. Baklanov, M. R., Mogilnikov, K. P., Polovinkin, V. G., Dultsev, F. N. Determination of pore size distribution in thin films by ellipsometric porosimetry *Journal of Vacuum Science & Technology B* **2000**, 18, 1385-1391

32. Horcajada, P., Ramila, A. Perez-Pariente, J., Vallet-Regi, M. Influence of pore size of MCM-41 matrices on drug delivery rate *Microporous Mesoporous Materials* **2004**, 68, 105–109.

33. Yang, Z., Mokaya, R. Probing the effect of the carbonisation process on the textural properties and morphology of mesoporous carbons. *Microporous and Mesoporous Materials* **2008**, 113, 378-384.

34. Ignat, M., Van Oers, C. J., Vernimmen, J., Mertens, M., Potgieter-Vermaak, S., Meynen, V., Popovici, E., et al. Textural property tuning of ordered mesoporous carbon obtained by glycerol conversion using SBA-15 silica as template. *Carbon* **2010**, 48 (5), 1609-1618.

Chapter 4

CONCLUSIONS AND FUTURE WORK

Highly ordered mesoporous materials have been of great interest in numerous applications such as catalysis, adsorption, energy storage, and drug delivery systems due to the ability to tailor morphological characteristics to accommodate selectively sized molecules. Nanocasting procedure using hard-templates to synthesize ordered mesoporous materials has been a well-known method but since it is an obviously elaborate and expensive process, soft supramolecular self-assembly is desirable. This research work utilized soft templating to generate mesoporous carbon film materials with different pore size and structure as host for drug uptake and controlled release. In order to modify the morphological properties of the film, pore swelling agents and different structure-directing agents are incorporated in the synthesis pathway to control the pore size and structure. The resulting carbon films FDU15, FDU16, and PS-PEO possesses varying pore sizes from 1.4nm, 2nm, and 6nm, respectively. Also, FDU15 forms two-dimensional (2D) hexagonal packing while FDU16 and PS-PEO generate cubic mesostructures. In addition to pore size and structure, hydrophobicity is also investigated by varying the carbonization temperatures of FDU16 films from 600°C, 800°C, and 1000°C. These films are evaluated using Mitoxantrone dihydrochloride as the model drug for adsorption and release studies.

First, to be able to control the pore size, homopolymer polystyrene (hPS) is introduced to the phenolic resin/poly(styrene-block-ethylene oxide) (SEO) as a pore expander. Significant differences in morphology and pore expansion are observed for the thin films in comparison to previously reported bulk powder

using the same system. Porosity of the PS-PEO films is nearly independent of the swelling agent content for addition of up to 10% hPS. This effect is attributed to surface segregation of the hPS which subsequently decreased the hPS concentration in the hydrophobic domains. The templated films yield narrow pore size distribution for <10% hPS and eventually broadens and shift to larger pore sizes thereafter. Elliptical pores are also observed and film contraction increases with hPS loading. The latter is contrary to results reported in powders wherein increasing hPS addition can restrain mesostructural shrinkage. This behavior can be elucidated by the process happening during carbonization in which films experience uniaxial contraction compared to the isotropic phenomena in powders. Moreover, poor ordering is observed compared to powders even though the molecular weight of the SEO is an order magnitude smaller for the film. We hypothesized that the poor order is attributed to rapid vitrification during spin coating and the crosslinking of the phenolic resin being faster than the template can re-organize into a highly ordered structure.

Results from the Mitoxantrone dihydrochloride drug uptake showed that loading capacity for the 2nm pore cubic film FDU-16-800 (2.62 $\mu g/cm^2$) is independent of its thickness, which can suggest that adsorption is beneath the film surface. Additionally, hexagonally packed FDU-15-800 film is able to adsorb more (3.03 $\mu g/cm^2$) possibly due to the filling up of the long cylindrical pores. In terms of the release, comparing the 2nm cubic FDU-16-800 and 1.4nm hexagonal FDU-15-800, both had an initial burst (~20% for the drug loaded) then followed by controlled release with FDU-16-800 having the highest amount of drug desorbed (1.45 $\mu g/cm^2$) after 2 weeks; this is only 56% of the drug loaded. FDU-15-800 was able to release about 30% which was expected since the pore size is

relatively small and are oriented parallel to the substrate which limits the number of accessible pores. The orientation of the pores is a contributing factor to the release kinetics as it would be easier to release if the pores were accessible through the top surface as opposed to just the sides of the film. Also, considering that FDU-15-800 have long cylindrical pores, it will take a longer time for the adsorbed molecules to travel along this path and reach the aqueous solution compared to molecules that are present near the surface.

Comparison of the cubic films FDU-16-800 (2nm) and PS-PEO-800 (5nm), the latter manifested the highest uptake (3.5μg/cm^2) primarily because of its large pore size that provided a larger internal volume to accommodate more molecules. However, presence of large pores in PS-PEO-800 films did not directly translate to a faster release rate. It is still unclear on what the contributing factor is for this behavior as previous reports on the effect of pore size to drug release have shown different results too. In a study done on MCM-41, the larger pore size material obtained from C_{16}TAB, showed 68% release as opposed to only 55% for the smaller pore size counterpart obtained from C_{12}TAB [Vallet-Regi et al , 2004]. Furthermore, Vallet-Regi and co-workers evaluated MCM-48 molecular sieves with Ia3d symmetry and pore size of 3.6nm, as well as LP-Ia3d, which possesses the same symmetry but exhibits a larger pore size of 5.7nm. The IBU release rate was found faster from LP-Ia3d indicative of the pore-size effect is also present on this ordering. Andersson et al (2004) considered that apart from pore-size effect, additional factors such as pore connectivity, geometry, and matrix degradation in aqueous media can influence the kinetic of release. On the other hand, work done by Qu et al (2006) for the release of captopril from several 2D hexagonal structures suggested that the

pore-size effect can be evaluated only if the morphology is similar at the microstructure level. However, for non-eroding nanoporous templates in the form of anodic aluminum oxide (AAO) with 20nm and 200nm pore sizes, the monitored Doxorubicin release after 2 weeks was reported to be approximately 30% and 20%, respectively [Gultepe, 2010]. Details on the apparent difference in release as a function of the pore size was not explicitly elucidated but they mentioned that this behavior is described by an activated surface-density-dependent desorption model; the fewer the number of drug molecules left on the surface, the faster the release rate. Hence, they reported that the release profile is determined not only by the drug-surface interaction but also by the interaction between the drug molecules.

For the analyzed samples, even if FDU-16-800 and PS-PEO-800 both possess cubic structures, they cannot be directly compared due to the fact that different templates were used during the synthesis process, poly(ethylene oxide)-block-poly(propylene oxide)-block-poly(ethylene oxide) (PEO-PPO-PEO) and poly(styrene-block-ethylene oxide) SEO, respectively. This may contribute to a difference to the morphology at the microstructure level. Moreover, atomic force microscope (AFM) micrograph of the PS-PEO-800 appears to have corrugated features. This surface profile could have contributed to the retarded release rate. To better understand the pore-size effect for these materials, additional experiments should be conducted using the set of PS-PEO materials with pore sizes that were systematically varied through the addition of hPS. Since these are templated carbons using the same SEO structure-directing agent, comparison between films is possible and the analysis of the release as a function of pore size can be better explained.

Additionally, effect of film hydrophobicity to drug release was also investigated. Varying the carbonization temperature changes the hydrophobicity of the film as the mesoporous polymers gradually transforms to carbon frameworks by the process of dehydrogenation. The surface hydrophobicity impacts the fraction of drug release with a decrease from 78% to 43%, as the films become more hydrophobic when carbonized at higher temperatures. This is consistent with previous study wherein modification of the mesoporous material with long alkyl chains increased the surface hydrophobicity [Doadrio et al, 2006] thereby inhibited the drug due to the presence of hydrophobic interactions between the drug and the surface and a decrease in the wettability of the surface by the aqueous solution.

The results from this research work are able to provide an insight on how the pore orientation and surface characteristics impact drug loading and release performance of mesoporous carbon films. However, there are still some areas that need to be studied further: evaluation of additional loading/release parameters, surface modification, and biocompatibility for nanoporous coating/implant applications. Chapter 3 was able to present the loading capacity of each of the different materials analyzed; however, process parameters such as loading temperature and shaker speed can be incorporated to understand the impact of other factors in the drug loading procedure apart from the materials standpoint. This may provide additional information to assess what other factors to consider in maximizing drug loading capacity. In addition, evaluation of the materials synthesized from chapter 2, templated PS-PEO films added with hPS, to have a better understanding of the pore size effect on release for these type of materials is proposed too.

The ability to modify the film surfaces caters a broader range of guest molecules and can be tailored for use in specific applications. Pore wettability, surface hydrophobicity, and hydrophilicity depend on the functional group present and determine incursion of reactants in the mesopore domains [Stein, Andreas et al, 2009]. Carbon materials produced by high temperature carbonization are usually hydrophobic and this type of surface hydrophobicity modification is utilized as discussed in chapter 3, however, at higher temperatures films tend to experience mesostructural shrinkage, so to preserve the framework, it is then proposed to do an alternate method to modify the surface. To achieve superhydrophobic properties, fluorination can be employed. Other methods such as surface oxidation, sulfonation, or introduction of other charged groups could also make the pore surfaces more accessible to polar fluids. The most commonly used oxidant for carbonaceous materials is an aqueous solution of either concentrated or diluted nitric acid. Nitric acid oxidation is a highly efficient process for generating surface functional groups, and is quite controllable, simply by tuning the acid concentration, temperature, and treatment duration. In the future, thorough understanding of the factors that influence loading and release performance of mesoporous films will be beneficial in determining the appropriate systems for drug delivery.

Apart from Mitoxantrone dihydrochloride used as the model drug in the experiments, utilizing different sized host molecules or biologically active materials can also be an area to look into to determine viability for other applications such as in implant systems for tissue engineering. Studies have shown that porous materials developed for use as scaffolds for cell growth is of particular interest in tissue engineering and regenerative medicine because it can

be potentially tailored to mimic the natural extracellular matrix (ECM) [Ferrer et al, 2008]. The natural ECMs in the body are mainly composed of extracellular macromolecules classified as proteoglycans and fibrous proteins with diameters ranging from 50 to 150nm, depending on the tissue type [Elsdale and Bard, 1972]. Reports also showed that cells attachment and proliferation were found to be good on micro and nanostructured materials as topographic features can affect the cell behavior [Teixeira, et al, 2003]. Thus, biocompatible materials processed with suitable morphology can potentially serve as scaffolds. Moreover, there had been published work on carbon meshes used in tissue engineering which have mostly been prepared from carbon fibers and nanotubes (CNT), both single wall (SWCNT) and multi-wall (MWCNT) [Ferrer et al, 2008]. A study conducted on scaffolds composed of MWCNT and chitosan (CHI), with well-defined microchannel porous structure, for development of osteoblast lineage using myoblastic mouse cell and recombinant bone morphogenetic protein-2 (BMP-2) has been reported [Abarrategi, et al, 2007]. In vivo and in vitro results suggested that these materials can be biocompatible and biodegradable supports for cell growth. In addition, Sabata et al (2009) demonstrated biocompatibility of hydrogenated amorphous carbon films for stem cell culture. As such, it is interesting to evaluate mesoporous carbon/chitosan films as nanoporous coatings or to serve as scaffolds for implant applications in tissue engineering.

REFERENCES

Baklanov, M. R., Mogilnikov, K. P., Polovinkin, V. G., Dultsev, F. N. Determination of pore size distribution in thin films by ellipsometric porosimetry *Journal of Vacuum Science & Technology B* **2000**, 18, 1385-1391.

Barton, T. J.; Bull, L. M.; Klemperer, W. G.; Loy, D. A.; McEnaney, B.; Misono, M.; Monson, P. A.; Pez, G.; Scherer, G. W.; Vartuli, J. C.; Yaghi, O. M. Tailored Porous Materials *Chemistry of Materials* **1999**, *11*, 2633.

Bates, F. S.; Fredrickson, G. H. Block Copolymers - Designer Soft Materials *Physics Today* **1999**, *52*, 32.

Beck, J. S., Vartuli, J. C., Roth, W. J., Leonowicz, M. E. Kresge, C. T., Schmitt, K. D., Chu, C. T. W., Olson, D. H., Sheppard, E. W. A new family of mesoporous molecular sieves prepared with liquid crystal templates *Journal of the American Chemical Society* **1992** 114 (27), 10834-10843.

Blin, J. L.; Otjacques, C.; Herrier, G.; Su, B. L. Pore Size Engineering of Mesoporous Silicas Using Decane as Expander *Langmuir* **2000**, *16*, 4229.

Brinker, C. J.; Dunphy, D. R. Morphological Control of Surfactant-Templated Metal Oxide Films Current Opinion in Colloid & Interface Science 2006, 11, 126.

Brinker, C. J.; Lu, Y. F.; Sellinger, A.; Fan, H. Y. Evaporation-Induced Self-Assembly: Nanostructures Made Easy *Advanced Materials* **1999**, *11*, 579.

Cao, L.; Man, T.; Kruk, M. Synthesis of Ultra-Large-Pore SBA-15 Silica with Two-Dimensional Hexagonal Structure Using Triisopropylbenzene As Micelle Expander *Chemistry of Materials* **2009**, *21*, 1144.

Cavicchi, K. A.; Russell, T. P. Solvent Annealed Thin Films of Asymmetric Polyisoprene-Polylactide Block Copolymers *Macromolecules* **2007**, *40*, 1181.

Chen, L., Zhu, G., Zhang, D., Zhao, H., Guo, M., Shi, W., Qiu, S. Novel mesoporous silica spheres with ultra-large pore sizes and their application in protein separation J. Mater. Chem. 19 (2009) 2013-2017.

Cheng, S.-H.; Lee, C.-H.; Chen, M.-C.; Souris, J. S.; Tseng, F.- G.; Yang, C.-S.; Mou, C.-Y.; Chen, C.-T.; Lo, L.-W. Tri-Functionalization of Mesoporous Silica Nanoparticles for Comprehensive Cancer Theranostics-the Trio of Imaging, Targeting and Therapy. *Journal of Materials Chemistry* **2010**, 20, 6149-6157.

Cho, K., Wang, X., Nie, S., Chen, Z., Shin, D. Therapeutic Nanoparticles for Drug Delivery in Cancer *Clinical Cancer Research* **2008**, 14, 1310-1316.

Corma, A. From Microporous to Mesoporous Molecular Sieve Materials and Their Use in Catalysis. *Chemical Reviews* **1997**, 97, 2373-2420.

Dai, K. H.; Kramer, E. J.; Shull, K. R. Interfacial segregation in two-phase polymer blends with diblock copolymer additives: the effect of homopolymer molecular weight *Macromolecules* **1992**, *25*, 220.

Deng, Y., Yu, T., Wan, Y., Shi, Y., Meng, Y., Gu, D., Zhang, L., Huang, Y., Liu, C., Wu, X., Zhao, D. Ordered Mesoporous Silicas and Carbons with Large Accessible Pores Templated from Amphiphilic Diblock Copolymer Poly(ethylene oxide)-b-polystyrene *Journal American Chemical Society* **2007**, 129, 1690-1697

Deng, Y., Liu, J., Liu, C., Gu, D., Sun, Z., Wei, J., Zhang, J., Zhang, L., Tu, B., Zhao, D. Ultra-Large-Pore Mesoporous Carbons Templated from Poly(ethylene oxide)-b-Polystyrene Diblock Copolymer by Adding Polystyrene Homopolymer as a Pore Expander *Chem. Mater.* **2008**, 20, 7281–7286

Derylo-Marczewska, A.; Marczewski, A. W.; Skrzypek, I.; Pikus, S.; Kozak, M. Effect of Addition of pore expanding agent on changes of structure of ordered mesoporous characteristics silicas *Applied Surface Science* **2008**, *255*, 2851.

Doadrio, J. C., Sousa, E. M. B., Izquierdo-Barba, I., Doadrio, A. L., Perez-Pariente, J., & Vallet-Regí, M. Functionalization of mesoporous materials with long alkyl chains as a strategy for controlling drug delivery pattern. *Journal of Materials Chemistry* **2006**, *16*(5), 462.

Elsdale T, Bard J. Collagen substrata for studies on cell behavior. Journal of Cell Biology **1972**, 54, 626–37.

Fan, J.; Yu, C.; Lei, J.; Zhang, Q.; Li, T.; Tu, B.; Zhou, W.; Zhao, D.Low-Temperature Strategy to Synthesize Highly Ordered Mesoporous Silicas with Very Large Pores *J. Am. Chem. Soc.* **2005**, *127*, 10794.

Fang, Y., Gu, D., Zou, Y., Wu, Z., Li, F., Che, R., Deng, Y., Tu, B. and Zhao, D., A Low-Concentration Hydrothermal Synthesis of Biocompatible Ordered Mesoporous Carbon Nanospheres with Tunable and Uniform Size. *Angewandte Chemie International Edition* **2010**, 49: 7987–7991.

Farrell, S., Hesketh, R., Savelski, M., Slater, C. Fundamentals, Design and Applications of Drug Delivery Systems 2003 American Society for Engineering Education Annual Conference and Exposition Session 1313

Feng, D.; Lv, Y.; Wu, Z.; Dou, Y.; Han, L.; Sun, Z.; Xia, Y.; Zheng, G.; Zhao, D. Free-Standing Mesoporous Carbon Thin Films with Highly Ordered Pore Architectures for Nanodevices *Journal of the American Chemical Society* **2011**, *133*, 15148.

Gu, J. Su, S. Li, Y., He, Q., Shi, J., Hydrophilic mesoporous carbon nanoparticles as carriers for sustained release of hydrophobic anti-cancer drugs *Chemical Communications* **2011**, 47, 2101-2103

Gultepe E, Nagesha D, Casse BD, Banyal R, Fitchorov T, Karma A, Amiji M, Sridhar S. Sustained Drug Release from Non-eroding Nanoporous Templates *Small* **2010**, 6, 213-216.

Hadmack, M. Bragg diffraction from a cubic crystal lattice http://en.wikipedia.org/wiki/File:Bragg_diffraction.png Downloaded 18 October 2011.

Holland, B. T.; Blanford, C. F.; Stein, A. Synthesis of Macroporous Minerals with Highly Ordered Three-Dimensional Arrays of Spheroidal Voids *Science* **1998**, *281*, 538.

Horcajada, P., Ramila, A. Perez-Pariente, J., Vallet-Regi, M. Influence of pore size of MCM-41 matrices on drug delivery rate *Microporous Mesoporous Materials* **2004**, 68, 105–109.

Hudson, S.; Cooney, J.; Magner, E. Proteins in mesoporous silicates *Angewandte Chemie-International Edition* **2008**, *47*, 8582.

Ignat, M., Van Oers, C. J., Vernimmen, J., Mertens, M., Potgieter-Vermaak, S., Meynen, V., Popovici, E., et al. Textural property tuning of ordered mesoporous carbon obtained by glycerol conversion using SBA-15 silica as template. *Carbon* **2010**, 48 (5), 1609-1618.

Jia G, Wang H, Yan L, Wang X, Pei R, Yan T. Cytotoxicity of carbon nanomaterials: single-wall nanotube, multi-wall nanotube and fullerene. Environ Sci Technol 2005, 39, 1378–83.

Jin, S., Ye, K., Nanoparticle-Mediated Drug Delivery and Gene Therapy *Biotechnology Progress* **2007**, 23, 32–41

Kim, G.; Libera, M. Morphological Development in Solvent-Cast Polystyrene–Polybutadiene–Polystyrene (SBS) Triblock Copolymer Thin Films *Macromolecules* **1998**, *31*, 2569.

Kim, T., Chung, P., Slowing, I., Tsunoda, M., Yeung, E., Lin, V. Structurally Ordered Mesoporous Carbon Nanoparticles as Transmembrane Delivery Vehicle in Human Cancer Cells *Nano Letters* **2008**, 8 (11), 3724–3727.

Kruk, M.; Cao, L. Pore Size Tailoring in Large-Pore SBA-15 Silica Synthesized in the Presence of Hexane *Langmuir* **2007**, *23*, 7247.

Le Page, M., Beau, R. Duchene, J., Porous silica particles containing a crystallized phase and method Application No. US 3493341D A filed on 23-Jan-1967; Publication No. US 3493341 A published on 03-Feb-1970

Lee, J.; Yoon, S.; Hyeon, T.; Oh, S. M.; Kim, K. B. Synthesis of a new mesoporous carbon and its application to electrochemical double-layer capacitorsChem. Commun.**1999**, 2177.

Lee, K.T., Lytle, J.C., Ergang, N.S., Oh, S.M. & Stein, A. Synthesis and Rate Performance of Monolithic Macroporous Carbon Electrodes for Lithium-Ion Secondary Batteries. *Advanced Functional Materials* **15**, 547-556 (2005)

Li, Y., Chen, X. & Gu, N. Computational investigation of interaction between nanoparticles and membranes: hydrophobic/hydrophilic effect. *The Journal of Physical Chemistry B* **2008,** 112, 16647-16653.

Liang, C. D.; Hong, K. L.; Guiochon, G. A.; Mays, J. W.; Dai, S. Synthesis of a Large-Scale Highly Ordered Porous Carbon Film by Self-Assembly of Block Copolymers. *Angewandte Chemie-International Edition* **2004**, *43*, 5785.

Lin, E. K.; Kolb, R.; Satija, S. K.; Wu, W. L. Reduced Polymer Mobility near the Polymer/Solid Interface as Measured by Neutron Reflectivity *Macromolecules* **1999**, *32*, 3753.

Liang, C. D.; Dai, S. Synthesis of Mesoporous Carbon Materials via Enhanced Hydrogen-Bonding Interaction *Journal of the American Chemical Society* **2006**, *128*, 5316.

Liang, C.; Li, Z.; Dai, S. Mesoporous carbon materials: Synthesis and modification. *Angewandte Chemie-International Edition* **2008,** *47* (20), 3696-3717.

Lu, J., Liong, M., Zink, J. and Tamanoi, F. Mesoporous Silica Nanoparticles as a Delivery System for Hydrophobic Anticancer Drugs. *Small* **2007**, 3, 1341–1346.

Lu, R., Shi, Y., Wan, Y., Weng, Y., Zhang, F., Gu, D., Chen, Z., Tu. B., Zhao, D.. Triconstituent Co-assembly to Ordered Mesostructured Polymer-Silica and Carbon-Silica Nanocomposites and Large-Pore Mesoporous Carbons with High Surface Areas *Journal of the American Chemical Society* **2006**, 128, 11652-11662.

Meng, Y., Gu, D., Zhang, F., Shi, Y., Cheng, L., Feng, D., Wu, Z., Chen, Z., Wan, Y., Stein, A., Zhao, D. A Family of Highly Ordered Mesoporous Polymer Resin and Carbon Structures from Organic-Organic Self-Assembly *Chemistry of Materials* **2006**, 18, 4447-4464

Meng, Y.; Gu, D.; Zhang, F. Q.; Shi, Y. F.; Yang, H. F.; Li, Z.; Yu, C. Z.; Tu, B.; Zhao, D. Y. Ordered Mesoporous Polymers and Homologous Carbon Frameworks: Amphiphilic Surfactant Templating and Direct Transformation. *Angewandte Chemie-International Edition* **2005**, *44*, 7053.

Moghimi, S.M., Hunter, A.C., and Andresen, T.L. Factors Controlling Nanoparticle Pharmacokinetics: An Integrated Analysis and Perspective *Annual Review of Pharmacology and Toxicology* **2012**, 52, 481-503.

Moghimi SM, Szebeni J. Stealth liposomes and long circulating nanoparticles: critical issues in phar- macokinetics, opsonization and protein-binding properties. *Prog Lipid Res* **2003**, 42, 463-478.

Moriguchi, I.; Ozono, A.; Mikuriya, K.; Teraoka, Y.; Kagawa, S.; Kodama, M. Micelle-templated mesophases of phenol-formaldehyde polymer. *Chemistry Letters* **1999,** (11), 1171-1172.

Nicole, L.; Boissiere, C.; Grosso, D.; Quach, A.; Sanchez, C. Mesostructured hybrid organic–inorganic thin films *Journal of Materials Chemistry* **2005**, *15*, 3598.

Ochekpe, N. A., Olorunfemi, P. O., & C, N. Nanotechnology and Drug Delivery Part 1 : Background and Applications. *Tropical Jounal of Pharmaceutical Research* **2009**, *8*, 265-274.

Oh, J-K., Drumright, R., Siegwart, D., Matyjaszewski, K. The development of microgels/nanogels for drug delivery applications *Progress in Polymer Science* **2008**, 33, 448–477.

Pan, K., Zhou, W., Tian, G., Pan, Q., Tian, C., Xie, T., Dong, Y., Wang, D., Fu, H. Dye-Sensitized Solar Cells Based on Large-Pore Mesoporous TiO2 with Controllable Pore Diameters *European Journal of Inorganic Chemistry Eur. J. Inorg. Chem.* **2011** (30) 4730-4737.

Paolino, Donatella, et.al., *Drug Delivery Systems*. Encyclopedia of Medical Devices and Instrumentation, Second Edition, **2006** John Wiley & Sons, Inc.

Ryoo, R.; Joo, S. H.; Kruk, M.; Jaroniec, M. Ordered mesoporous carbons. *Advanced Materials* **2001,** *13* (9), 677-681.

Ryoo, R., Hoon Joo, S., Jun, S. Synthesis of Highly Ordered Carbon Molecular Sieves via Template-Mediated Structural Transformation *The Journal of Physical Chemistry B* **1999**, 103 (37), 7743-7746.

Sanchez, C.; Boissiere, C.; Grosso, D.; Laberty, C.; Nicole, L. Design, Synthesis, and Properties of Inorganic and Hybrid Thin Films Having Periodically Organized Nanoporosity *Chemistry of Materials* 2008, *20*, 682.

Schuth, F. Non-siliceous Mesostructured and Mesoporous Materials *Chemistry of Materials* **2001**, *13*, 3184.

Segalman, R. A. Patterning with Block Copolymer Thin Films *Materials Science & Engineering R-Reports* **2005**, *48*, 191.

Schuster, J.; Koehn, R.; Keilbach, A.; Doeblinger, M.; Amenitsch, H.; Bein, T. Two-Dimensional-Hexagonal Periodic Mesoporous Polymer Resin Thin Films by Soft Templating. *Chemistry of Materials* **2009**, *21*, 5754.

Shull, K. R.; Winey, K. I. Homopolymer Distributions in Lamellar Copolymer/Homopolymer Blends *Macromolecules* **1992**, *25*, 2637.

Si-Han Wu, Yann Hung and Chung-Yuan Mou Mesoporous silica nanoparticles as nanocarriers Chem. Commun**.**, **2011**, **47**

Smith, F. W. Optical constants of a hydrogenated amorphous carbon film *Journal of Applied Physics* **1984**, *55*, 764.

Sokolsky-Papkov, M., Agashi, K., Olaye, A., Shakesheff, K., Domb, A. Polymer carriers for drug delivery in tissue engineering *Advanced Drug Delivery Reviews* **2007**, 59, 187–206.

Song, L.; Feng, D.; Campbell, C. G.; Gu, D.; Forster, A. M.; Yager, K. G.; Fredin, N.; Lee, H.-J.; Jones, R. L.; Zhao, D.; Vogt, B. D. Robust conductive mesoporous carbon–silica composite films with highly ordered and oriented orthorhombic structures from triblock-copolymer template co-assembly *Journal of Materials Chemistry* **2010**, *20*, 1691.

Song, L., Feng, D., Fredin, N., Yager, K., Jones, R., Wu, Q., Zhao, D., Vogt, B.. Challenges in Fabrication of Mesoporous Carbon Films with Ordered Cylindrical Pores via Phenolic Oligomer Self- Assembly with Triblock Copolymers *ACS Nano* **2010**, 4, 189–198

Song, L.; Feng, D.; Lee, H.-J.; Wang, C.; Wu, Q.; Zhao, D.; Vogt, B. D. Stabilizing surfactant templated cylindrical mesopores in carbon films through composite formation with silica reinforcement *Journal of Physical Chemistry C* **2010**, *114*, 9618

Stein, A. Advances in Microporous and Mesoporous Solids—Highlights of Recent Progress.*Advanced Materials* **2003**, *15*, 763.

Stein, G. E.; Cochran, E. W.; Katsov, K.; Fredrickson, G. H.; Kramer, E. J.; Li, X.; Wang, J. Symmetry breaking of in-plane order in confined copolymer mesophases *Physical Review Letters* **2007**, *98*.

Suh, M., Lee, H., Park, J., Lee, U., Kwon, Y., Kim, D.. A Mesoporous Silica Thin Film as Uptake Host for Guest Molecules with Retarded Release Kinetics *A European Journal of Chemical Physics and Physical Chemistry* **2008**, 9, 1402 – 1408.

Tanaka, S.; Katayama, Y.; Tate, M. P.; Hillhouse, H. W.; Miyake, Y. Fabrication of continuous mesoporous carbon films with face-centered orthorhombic symmetry through a soft templating pathway *Journal of Materials Chemistry* **2007**, *17*, 3639.

Tanaka, S.; Nishiyama, N.; Egashira, Y.; Ueyama, K. Synthesis of ordered mesoporous carbons with channel structure from an organic-organic nanocomposite. *Chemical Communications* **2005,** (16), 2125-2127.

Teixeira AI, Abrams GA, Bertics PJ, Murphy CJ, Nealey PF. Epithelial contact guidance on well-defined micro- and nanostructured substrates. Journal of Cell Science 2003, 116, 1881–92.

Tian Yu, Alexander Malugin, and Hamidreza Ghandehar Impact of Silica Nanoparticle Design on Cellular Toxicity and Hemolytic Activity *ACS Nano*, **2011**, 5 (7), pp 5717–5728

Torchilin, V. P. Nanoparticulates as drug carriers. Imperial College Press, 2006. London.

Torchilin VP. Targeted Pharmaceutical Nanocarriers for Cancer Therapy and Imaging *AAPS Journal* **2007**, 9(2), Article 15.

Trewyn, B., Giri, S., Slowing, I., Lin, V. Mesoporous silica nanoparticle based controlled release, drug delivery, and biosensor systems *Chemical Communications* **2007**, 3236–3245

Tsai, C.-P.; Chen, C.-Y.; Hung, Y.; Chang, F.-H.; Mou, C.-Y. Monoclonal Antibody-Functionalized Mesoporous Silica Nanoparticles (MSN) for Selective Targeting Breast Cancer Cells. *Journal of Materials Chemistry* **2009**, 19, 5737–5743.

Vallet-Regí, M., Balas, F. and Arcos, D. Mesoporous Materials for Drug Delivery. Angewandte Chemie International Edition **2007**, 46: 7548–7558

Vinu, A.; Miyahara, M.; Ariga, K. Biomaterial Immobilization in Nanoporous Carbon Molecular Sieves: Influence of Solution pH, Pore Volume, and Pore Diameter *Journal of Physical Chemistry B* **2005**, *109*, 6436.

Vogt, B. D.; Chavez, V. L.; Dai, M.; Arreola, M. R. C.; Song, L.; Feng, D.; Zhao, D.; Perera, G. M.; Stein, G. E. Impact of film thickness on the morphology of mesoporous carbon films using organic-organic self assembly *Langmuir* **2011**, *27*, 5607.

Wan, Y.; Shi, Y.; Zhao, D. Supramolecular Aggregates as Templates: Ordered Mesoporous Polymers and Carbons. *Chemistry of Materials* **2008**, *20*, 932.

Wan, Y. & Zhao, D. On the controllable soft-templating approach to mesoporous silicates. *Chemical Reviews* **2007**, 107, 2821-2860.

Wang, S. Ordered mesoporous materials for drug delivery *Microporous and Mesoporous Materials* **2009**, 117, 1–9.

Wang, X., Bozhilov, K.N. & Feng, P. Facile Preparation of Hierarchically Porous Carbon Monoliths with Well-Ordered Mesostructures. *Chemistry of Materials* **18**, 6373-6381 (2006).

Wang, X., Liu, P., Tian, Y. Ordered mesoporous carbons for ibuprofen drug loading and release behavior *Microporous and Mesoporous Materials* **2011**, 142, 334–340.

Wang, W., Wang, Y., Shi, H., Liu, H., Song, W. Self-assembled mesoporous carbon films for platinum metal catalyst loading *Thin Solid Films* **2010** (518) 3604–3609.

Watanabe, J. Iwamoto, S., Ichikawa, S. Entrapment of some compounds into biocompatible nano-sized particles and their releasing properties *Colloids and Surfaces B-Biointerfaces* **2005**, 42, 141–146.

Wisse E, Braet F, Luo D, et al. Structure and function of sinusoidal lining cells in the liver. *Toxicol Pathol* **1996**, 24, 100-111

Wu, S., Hung, Y. and Mou, C. Mesoporous silica nanoparticles as nanocarriers *Chemical Communications* **2011**, 47, 9972–9985.

Xia, Y. & Mokaya, R. Generalized and Facile Synthesis Approach to N-Doped Highly Graphitic Mesoporous Carbon Materials. *Chemistry of Materials* **17**, 1553-1560 (2005).

Xu, Z. P.; Zeng, Q. H.; Lu, G. Q.; Yu, A. B. Inorganic nanoparticles as carriers for efficient cellular delivery *Chemical Engineering Science* **2006**, 61 (3), 1027–1040.

Yan, A., Lau, B., Weissman, B., Külaots, I., Yang, N., Kane, A. and Hurt, R., Biocompatible, Hydrophilic, Supramolecular Carbon Nanoparticles for Cell Delivery. *Advanced Materials* **2006**, 18: 2373–2378.

Yang, C.-M., Weidenthaler, C., Spliethoff, B., Mayanna, M. & Schüth, F. Facile Template Synthesis of Ordered Mesoporous Carbon with Polypyrrole as Carbon Precursor. *Chemistry of Materials* **17**, 355-358 (2005).

Yang, Z., Mokaya, R. Probing the effect of the carbonisation process on the textural properties and morphology of mesoporous carbons. *Microporous and Mesoporous Materials* **2008**, 113, 378-384.

Yang, Z., Xia, Y., Sun, X. & Mokaya, R. Preparation and hydrogen storage properties of zeolite-templated carbon materials nanocast via chemical vapor deposition: effect of the zeolite template and nitrogen doping. *The Journal of Physical Chemistry B* **110**, 18424-18431 (2006).

Yiu, H., Botting, C., Botting, N., & Wright, P., Size selective protein adsorption on thiol-functionalised SBA-15 mesoporous molecular sieve *Phys. Chem. Chem. Phys.* **2001** (3) 2983-2985.

Yu, T., Malugin, A., Ghandehar, H. Impact of Silica Nanoparticle Design on Cellular Toxicity and Hemolytic Activity *ACS Nano* **2011**, 5 (7), 5717–5728.

Yuan, D-S., Zeng, J., Chen, J., Liu, Y. Highly Ordered Mesoporous Carbon Synthesized via in Situ Template for Supercapacitors *International Journal of Electrochemical Science* **2009** (4) 562 – 570.

Yuan, F., Dellian, M., Fukumura, D., et al. Vascular permeability in a human tumor xenograft: molecular size dependence and cutoff size. *Cancer Res* **1995**, 55, 3752-3756.

Zakhidov, A.A. et al. Carbon Structures with Three-Dimensional Periodicity at Optical Wavelengths. *Science* **282**, 897-901 (1998).

Zhao, D., Feng, J., Huo, Q., Melosh, N., Fredrickson, G., Chmelka, B., Stucky, G. Triblock Copolymer Syntheses of Mesoporous Silica with Periodic 50 to 300 Angstrom Pores *Science* **1998**, 297, 548-552.

Zhao, D., Huo, Q., Feng, J., Chmelka, B. F., Stucky, G. D. Nonionic Triblock and Star Diblock Copolymer and Oligomeric Surfactant Syntheses of Highly Ordered, Hydrothermally Stable, Mesoporous Silica Structures *J. Am. Chem. Soc.* **1998**, *120*, 6024

Zhao, Y., Sun, X., Zhang, G., Trewyn, B., Slowing, I., Lin, V. Interaction of Mesoporous Silica Nanoparticles with Human Blood Cell Membrane: Size and Surface Effects *ACS Nano* **2011**, 5 (2), 1366–1375.

Zhou, J., He, J., Zhang, C., Wang, T., Sun, D., Di, Z., & Wang, D.. Mesoporous carbon spheres with uniformly penetrating channels and their use as a supercapacitor electrode material. *Materials Characterization* **2010** 61(1), 31-38.

Zhu, S., Chen, C., Chen, Z., Liu, X., Li, Y., Shi, Y., Zhang, D. Thermo-responsive polymer-functionalized mesoporous carbon for controlled drug release *Materials Chemistry and Physics* **2011**, 126 (1-2), 357-363.

Zhuang, X., Wan, Y., Feng, C., Shen, Y., Zhao, D. Highly Efficient Adsorption of Bulky Dye Molecules in Wastewater on Ordered Mesoporous Carbons *Chemistry of Materials* **2009**, *21*, 706.